Available online at www.sciencedirect.com
ScienceDirect
C. R. Physique 8 (2007) 821–844
COMPTES RENDUS PHYSIQUE
http://france.elsevier.com/direct/COMREN/

Neutron scattering/Diffusion de neutrons

Small angle scattering from soft matter—application to complex mixed systems

François Boué [a,*], Fabrice Cousin [a], Jérémie Gummel [a], Julian Oberdisse [b], Géraldine Carrot [a], Abdeslam El Harrak [a]

[a] *Laboratoire Léon Brillouin, CEA–CNRS, Centre d'études de Saclay, 91191 Gif sur Yvette cedex, France*
[b] *Laboratoire des colloïdes, verres et nanomatériaux, Université Montpellier II, UMR 5587, 34095 Montpellier cedex 05, France*

Abstract

The advantage of small angle neutron scattering associated with isotopic labelling through deuteration is illustrated in the case of mixed systems, created by associating already well-known systems of characteristic structures; this is also important for applications. Our first mixed system associates charged polymer chains, polyelectrolytes (here polystyrene sulfonate, PSS), with oppositely charged particles, proteins (here lysozyme). Different fractions of deuterated water (D_2O) mixed with normal water are used to match the scattering length density of the protein or of the polymer in non-deuterated or deuterated version. First, this allows us to separate the protein and the polymer signal: we can then distinguish a case where the structures of each species alone in water are *hardly modified* by mixing, except for interconnections yielding a *gel*, and a case inducing *complete change* into a structure common to both species, made of *aggregated globules*. Second, using, for counterions of the polyions, deuterated TetraMethylAmmonium, together with matching both protein and polymer, we establish unambiguously the *counterion release* into the solvent. Third, matching only a fraction of polymer chains, the other being deuterated, we extrapolate at zero deuterated fraction their form factor and describe the chain conformation inside the complexes. Fourth, we illustrate the possibilities of modelling the signal on a second example of mixed system: a nanocomposite made of silica particles surrounded by polymer dispersed into a deuterated polymer matrix. Chains are then visible in such reinforced polymer system, in particular when it is submitted to elongation: we discuss a possible model for an ideal system, introducing the scattering contribution from deformed chains, another subject studied at LLB. ***To cite this article: F. Boué et al., C. R. Physique 8 (2007).***

Résumé

Diffusion de neutrons aux petits angles par la matière molle—application aux systèmes mixtes. Les possibilités de marquage par deutériation associées à la diffusion de neutrons aux petits angles sont illustrées dans le cas des systèmes mixtes, créés par l'association de systèmes simples aux structures caractéristiques connues dans le domaine de la matière molle ; ces systèmes mixtes sont très importants dans les applications. Le premier système choisi résulte du mélange de chaînes polymères chargées en solution dans l'eau (polyélectrolytes), ici du polystyrène sulfonate, avec des protéines de charge opposée, ici du lysozyme. Des mélanges eau lourde/eau légère à différents taux sont utilisés pour adapter la densité de longueur de diffusion du solvant à celle de la protéine ou du polymère. Ceci nous permet d'abord de séparer les signaux des deux espèces ; dans un cas, la répartition spatiale des deux composants est à peine modifiée, à l'exception de connexions menant à un gel, dans un autre un changement complet mène à une structure, partagée par les deux espèces, d'agrégats globulaires. Deuxièmement, en utilisant comme contre-ions des

* Corresponding author.
E-mail address: francois.boue@cea.fr (F. Boué).

1631-0705/$ – see front matter
doi:10.1016/j.crhy.2007.10.013

polyions, le TetraMethylAmmonium deutéré, nous démontrons sans ambiguïté le relargage des contre-ions dans le solvant. Troisièmement, en éteignant en même temps les signaux des protéines et des chaînes non deutérées, en présence d'une fraction de chaînes deutérées, nous pouvons extrapoler à fraction nulle le signal d'une seule chaîne et son facteur de forme, et en déduire sa conformation au sein des complexes. Finalement, nous illustrons les possibilités de modélisation sur un deuxième système mixte, un nanocomposite de particules de silice entourées par des chaînes polymères introduites dans une matrice polymère deutérée. Les chaînes sont alors visibles dans un tel système polymère renforcé, en particulier quand il est soumis à une élongation. Nous discutons un modèle possible qui introduit la diffusion anisotrope des chaînes et la "perte d'affinité", un autre sujet étudié au LLB.
Pour citer cet article : F. Boué et al., C. R. Physique 8 (2007).

Keywords: Small angle neutron scattering; Isotopic labelling; Deuteration; Matching; Deuterated water; Mixed systems; Polymer; Polyelectrolyte; Counterions; Chain conformation; Proteins; Gel; Aggregated globules; Silica particles; Nanocomposites; Modelling; Core–shell model; Deformed chains

Mots-clés : Diffusion de neutrons aux petits angles ; Marquage isotopique ; Deuteriation ; Adaptation de contraste ; Eau lourde ; Systèmes mixtes ; Polymère ; Polyélectrolyte ; Contre-ions ; Conformation des chaînes ; Protéines ; Gel ; Agrégats globulaires ; Particules de silice ; Nanocomposite ; Modélisation ; Modèle cœur–couronne ; Chaînes anisotropes

1. Introduction

The aim of this article is to give some examples of the possibilities of Small Angle Neutron Scattering developed recently in the field of soft matter, associated with labeling strategies. More general lectures on Small Angle Neutron Scattering can be found in several places [1–3]. Here, we present studies on polymers associated with a second species. The reason for this choice is that we want to illustrate the possibilities of SANS in the domain of mixed systems,[1] which is one of the most lively area of research at present. We now know enough about the behavior of single species systems, to feel encouraged to look at mixtures of these elements, which involve and mingle their specific properties into some new combinations. A large ensemble of the objects created under mixing involves the nanometer sizes measurable by Small Angle Scattering; this is true in particular when the wavelength order of magnitude of neutrons is concerned. Moreover, when looking at such mixtures with neutrons, the possibility of isotopic labeling is a very rich source of experiments. Labeling, mostly using deuterated solvent, or solute, allows us to play with contrast. This concept is explained below. At the same time, we chose here some examples in echo to the basic studies on polymer conformation developed some years ago in the pioneer "Groupe Polymères" of Saclay.

2. Small angles = large distances = low density fluctuations—contrast concept in SANS

We assume that the general expression for the elastic scattering in the kinematic approximation is already known:

$$\mathbf{I} = \sum_{\text{all nuclei}} b_i \exp(\mathrm{i}.\mathbf{q}.\mathbf{r}_\mathrm{i}). \sum_{\text{all nuclei}} b_j \exp(-\mathrm{i}.\mathbf{q}.\mathbf{r}_j) \tag{1}$$

where b_i (b_j) are the scattering lengths of nuclei i (j) located at spatial positions $\mathbf{r}_i$ ($\mathbf{r}_j$), and $\mathbf{q}$ is the scattering vector corresponding to a scattering angle θ, for an incoming beam of wavelength λ, with a modulus $q = (4\pi/\lambda)\sin(\theta/2)$.

Let us now focus on the specificity of Small Angle Scattering: the distances considered are large compared to interatomic distances. Thus we can group the atoms in 'elementary bricks' of repeating species: molecules, polymer chain repeating units.[2] We can even define as a continuous function $n_k(\mathbf{r})$, the number volume density of the species k at a point $\mathbf{r}$, so that the first term of the product above becomes:

$$\sum_{\text{all molecules } k} \int n_k(\mathbf{r})\, \mathrm{d}^3\mathbf{r} b_k \exp \mathrm{i}\mathbf{q}\mathbf{r} = \sum b_k.n_k(\mathbf{q}) \tag{2}$$

[1] We use 'mixed systems' as a probably imperfect translation of the French expression "Systèmes mixtes", widely used in the Soft Matter community.

[2] Chain units are sometimes called 'monomers', which is wrong: a monomer is a chemical species, of different formula, which reacts during the polymerization.

where $n_k(\mathbf{q})$ is the spatial Fourier transform of $n_k(\mathbf{r})$

$$I = \sum_{\text{species}} n_k(\mathbf{q}).\sum_{\text{species}} n_l(-\mathbf{q}) \tag{3}$$

where $n_{k(l)}(-\mathbf{q})$ is the conjugate of $n_{k(l)}(\mathbf{q})$.

Let us consider a system made of two molecular species, A and B. We have:

$$I = \big(b_A n_A(\mathbf{q}) + b_B n_B(\mathbf{q})\big).\big(b_A n_A(-\mathbf{q}) + b_B n_B(-\mathbf{q})\big) \tag{4}$$

Here comes a second important source of simplification related to distances large compared to interatomic distances, in condensed matter: the fact that the *density* fluctuations of the system are most of the time negligible. Hence $n_A(\mathbf{r})$ and $n_B(\mathbf{r})$ and the molar volumes v_A and v_B are linked by a simple relation:

$$v_A.n_A(\mathbf{r}) + v_B.n_B(\mathbf{r}) \sim \text{cst.} \tag{5a}$$

or in $\mathbf{q}$ space[3]

$$v_A n_A(\mathbf{q}) + v_B.n_B(\mathbf{q}) \sim \delta(\mathbf{q}) \equiv 0 \quad \text{at } \mathbf{q} \neq \mathbf{0} \tag{5b}$$

Replacing in (4), we get:

$$\begin{aligned} I(q) &= (b_A/v_A - b_B/v_B)^2.n_A(\mathbf{q}).n_A(-\mathbf{q}) \\ &= K_{AB}^2.n_A(\mathbf{q}).n_A(-\mathbf{q}) \end{aligned} \tag{6}$$

which depends only on $n_A(\mathbf{q})$ (or $n_B(\mathbf{q})$). One 'sees' the positional fluctuations of one species with respect to the other, since both positions are inter-related by the incompressibility relation: where species A is present, species B is not present. This is akin to the Babinet theorem in optics: the diffraction figure obtained for a given shape is the same when the shape corresponds to the transparent (e.g. cut out of a black cardboard) or the opaque part (e.g. black paint deposited on a transparent glass) of the planar object. The pendent of the difference between black and white is the contrast K_{AB}^2 in Eq. (6) above.

If we have more than two components, the incompressibility relation can be written

$$\sum b_k.n_k(\mathbf{q}) \sim \delta(\mathbf{q}) \equiv 0 \quad \text{at } q \neq 0 \tag{7}$$

If, for example we consider several species in a solvent, we can eliminate the solvent and obtain:

$$I = \sum_{k=A,B\ldots} (b_k/v_k - b_S/v_S)^2.n_k(\mathbf{q}).n_k(-\mathbf{q}) \tag{8}$$

which involves the density of contrast squared

$$K_{kS}^2 = (b_k/v_k - b_S/v_S)^2. \tag{9a}$$

We can then define ρ, a '*density of scattering length*'[4]

$$\rho_k = b_k/v_k \tag{9b}$$

Thus, all will depend on differences between values of ρ obtained for different molecules or other elementary bricks.

3. Deuteration: a superlabel

At this stage, remember that our reasoning is valid for any radiation, in particular photons, with two examples in practice:

[3] Rigorously, the limit at $q \to 0$ is $v_A n_A(q) + v_B.n_B(q) = k_B T.\ \chi_T$, where compressibility χ_T is negligible most of the time (completely opposite would be the case of CO_2 close to critical point, for example, where density fluctuations are huge).

[4] ρ is noted also N_b, in particular, in the neutron reflectivity community.

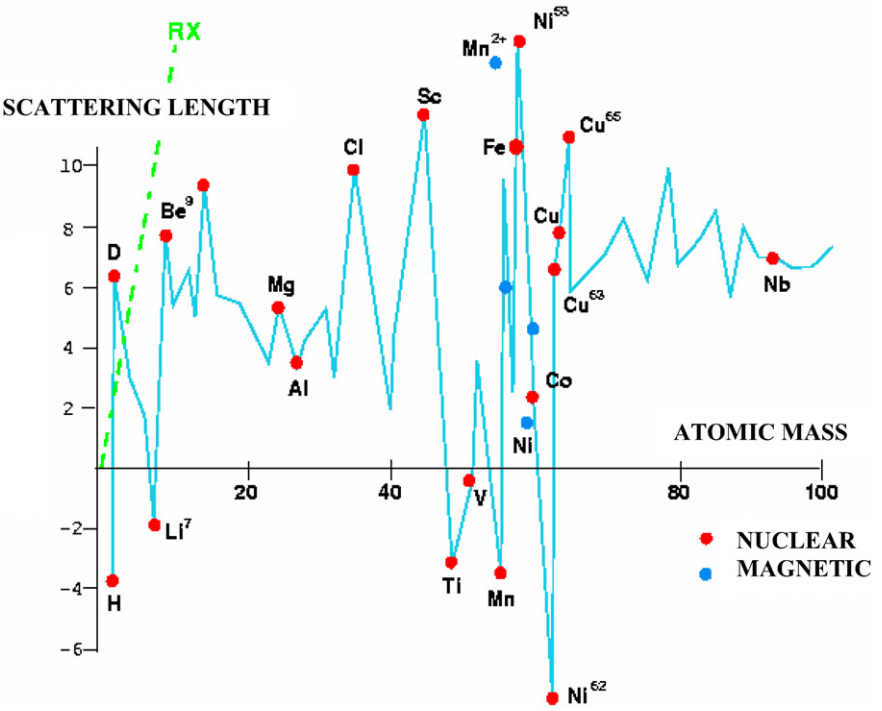

Fig. 1. Nuclear scattering length for thermal neutrons, b in 10^{-13} cm, versus the atomic mass (in dotted line is schematized the variation for X-rays which is linear in atomic number Z).

– usual, visible light as produced by lasers (e.g. red light or green light). In this case the contrast depends on differences in optical index;
– X-rays, where the contrast is proportional to the difference in electron density in the different electronic clouds of the atoms or molecules.

Let us, in particular, compare the neutron and X-ray cases in Fig. 1. We see that for neutrons, b displays a very erratic variation as a particles after purification. They were studied in solution, using on the nucleus, not on Z while for X-rays, it would be continuously increasing as a function of atomic number Z. As a consequence we can have a high difference of neutron scattering length densities between two nuclei of atoms, neighbours in values of Z, at variance with X-rays. Hence there is some 'contrast' between such neighbours which would be indistinguishable if one was using X-rays.

There is also a very important additional fact: *the isotopic effect*. When the nuclei are different for the same element, their interaction with neutrons is different. Let us look at the atomic number $Z = 1$: it corresponds to hydrogen (H), but also to deuterium (D), an isotope of hydrogen of very different scattering length, $b_D = 6.67$ fm instead of $b_H = -3.74$ fm. Let us evaluate the consequences of this on the value of ρ for water: we find 0.05×10^{-10} cm^{-2} for H_2O, instead of 6.6×10^{-10} cm^{-2} for D_2O.

The effect of replacing H by D on ρ for water will be similar for organic species where carbon C, which has about the same b value as oxygen, $b_C = 6.64$ fm, is combined with hydrogen in proportions similar to that for O in H_2O ('saturated' groups as in alkanes imply the group 'CH_2'). Many solvents are available in deuterated version, often because of their use in Nuclear Magnetic Resonance, which becomes here an 'objective ally' of neutron science. So just by replacing normal solvent by deuterated solvent, we can strongly increase the contrast of a non-deuterated solute. We can also create deuterated sequences in polymers, or in surfactants, via a convenient synthesis. Since the electronic clouds are not modified, neither chemical properties nor physicochemical interactions are strongly changed. This is particularly important for large objects, micelles, polymers, where the number N of individual molecules is large, which increases by the same factor N the enthalpy cost for mixing. For D and non-D polystyrene segments the enthalpy of mixing is χ_{HD}. $T = 10^{-4} k_B T$, which leads to $10^{-2} k_B T$ for a chain of 100 segments, and hence the

translational entropy of mixing ($\sim k_B T$ per chain) remains dominant. For segments of different chemical nature, the enthalpy of mixing would be around at least 100 times more, and would balance entropy, leading to phase separation between the two types of chains.

In summary, contrary to chemical labeling, deuteration is a thermodynamically neutral labelling in soft condensed matter because χ_{HD} is often small enough.

4. Playing with contrast

Now that we have defined the contrast, and know how to tune it, in particular through the use of deuterated species, we will show various uses of contrast and contrast matching.

4.1. Contrast variation

In order to use such possibilities at their best, we first need to know exactly the ρ value for each component. This is not so easy by calculation, because it requires knowing the species exact molecular volume, in the exact conditions of measurements, which is difficult to obtain accurately either from the literature or from densitometry. A simple way is to use neutrons: we realize a series of solvents of different ρ using different fractions ϕ_D of deuterated solvent, and measure for each species A the intensity scattered by a homogeneous solution of A in these solvents; the solution can be dilute, but can as well be a concentrated one. As long as the spatial distribution of species A stays the same for all fractions ϕ_D, only the front factor, i.e. the contrast K^2 will vary. Since K^2 will be a quadratic function of ϕ_D, we must find that $\sqrt{I}$ can be fitted by a linear function of ϕ_D. The zero value corresponds to a solvent having the same ρ than the solute A. In practice, we can class all species on an axis of scattering length density ρ (see Eq. (9b)), as shown for two examples in Fig. 2.

4.2. Ternary mixture: matching one species or the other in mixed systems: the case of polyelectrolyte–protein complexes

Here we consider two species A and B in a solvent S, with value ρ_A different enough from ρ_B. Then if we match one species with the appropriate mixture of deuterated (D) and non-deuterated (H) solvents, we have access to the contribution of the other species only. In the example which will be described here, our second species, B, is deuterated so it can be matched using a high D fraction, whereas species A is matched with a much lower D fraction. There is always a large contrast between the non-matched species (A or B) and the solvent matching the other species (B or A).

This strategy is very convenient for what is called a 'mixed system' (see Note 1 again). The interest is that such a system is very common in the field of soft matter, both on the synthetic/industrial side and on the biology/biotechnology side.

Among mixed systems, we will use as an example the one studied recently in detail at Laboratoire Léon-Brillouin [4–9], namely, complexes made by lysozyme, a positively charged protein in acid buffer (pH 4.7, 5×10^{-2} mol/L acetate buffer), and sodium poly(styrenesulfonate) (PSSNa), a negatively charged polyelectrolyte. This kind of 'mixed system' (protein and polyelectrolyte) has been very much studied macroscopically, and has many applications [10]. In this article, PSS is always used in its deuterated version D-PSS. In order to get either the PSSNa signal or the lysozyme signal independently, each PSS/protein composition has been achieved in two solvents: a fully D_2O buffer that matches (within less than 1%) the neutron scattering length density of deuterated PSSNa, and a 57%/43% H_2O/D_2O mixture that matches the neutron scattering length density of lysozyme.

This example is also an opportunity of showing a variety of different SANS signals often encountered in soft matter. Let us show a first case of complexes obtained for a *large excess* of polymer [4,5]. As a basis of comparison, let us describe the signal of a free protein at concentration low enough and ionic strength high enough that the differential scattering cross-section $d\Sigma/d\Omega$ is proportional to the scattering $S_1(q)$ of a single object. This is the continuous line in the log–log plot of Fig. 3: we see that it displays a plateau at low q, followed, when increasing q, by a smooth decay. This decay is described by the Guinier law:

$$S_1(q) \sim M_w.P(q) \sim M_w.\left(1 - q^2 R_g^2/3\right), \quad q R_g < 1 \tag{10}$$

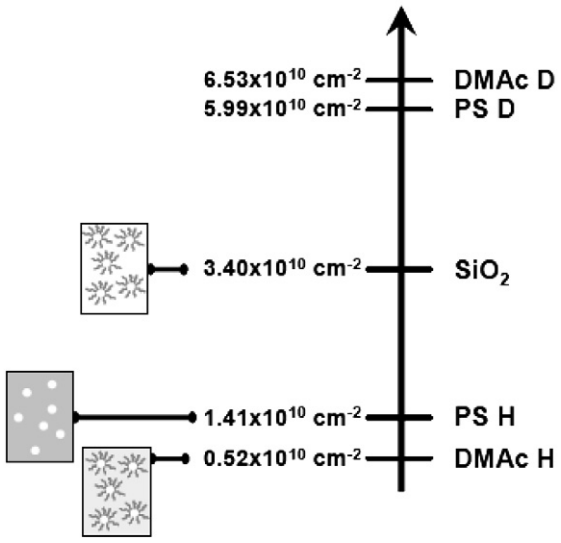

(a)

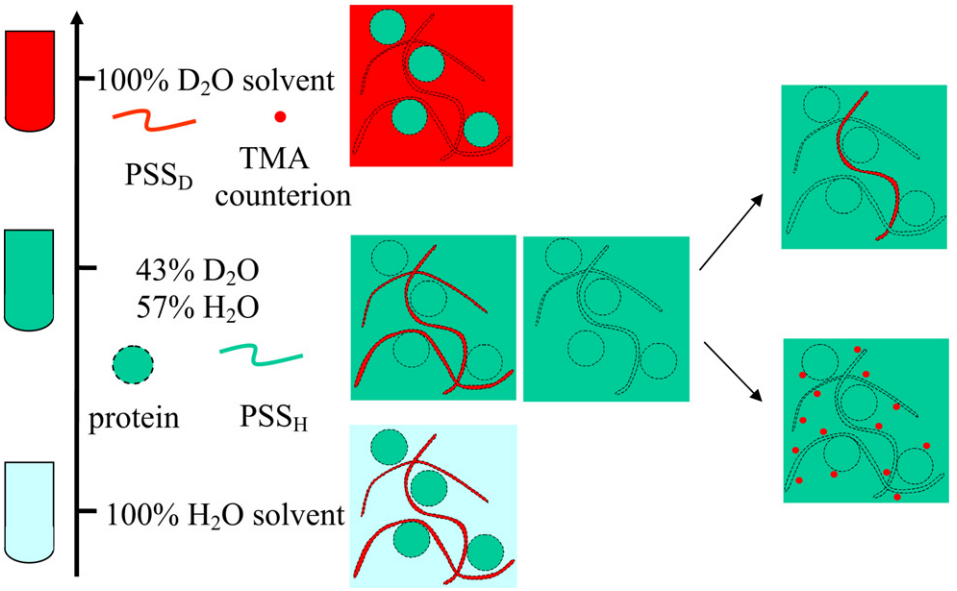

(b)

Fig. 2. (a) A first example of a scale for scattering length density for the system silica, DimethylAcetamide (DMAc) solvent in H (non-deuterated) and D (deuterated) versions, and polystyrene PS, in H and D version. (b) A second example of a scale for scattering length density for the system lysozyme (protein), sodium polystyrene sulfonate (PSS), deuterated (D) or not (H), TetraMethylAmmonium counterions (TMA^+), and the matching solvents.

where M_w is the weight average mass, $P(q)$ the form factor and R_g the radius of gyration. Increasing q even more and reaching $qR_g > 1$, we see that $P(q)$ decreases like q^{-4}. This 'Porod law' is characteristic of a compact object (no scattering from the inside of the object since it has a constant density) with a sharp interface with the solvent.

Let us compare it to the scattering of the protein inside the complex at high concentration of polyelectrolyte chains (+ symbols and o symbols in Fig. 3). At low q, we see also a Guinier law; a vertical shift has been introduced to make the free protein curve distinguishable, but, in reality, if it was just corrected to concentration, all curves would tend to the same zero q limit, because the protein keeps the same mass. On the contrary, at larger q the complexed protein scattering changes: it varies now as $q^{-1.7}$ instead of q^{-4}. Such variation is characteristic of an excluded volume chain as showed some time ago for polymer solutions by the Saclay Polymer Group [11]. A power law q^{-D_f} is expected

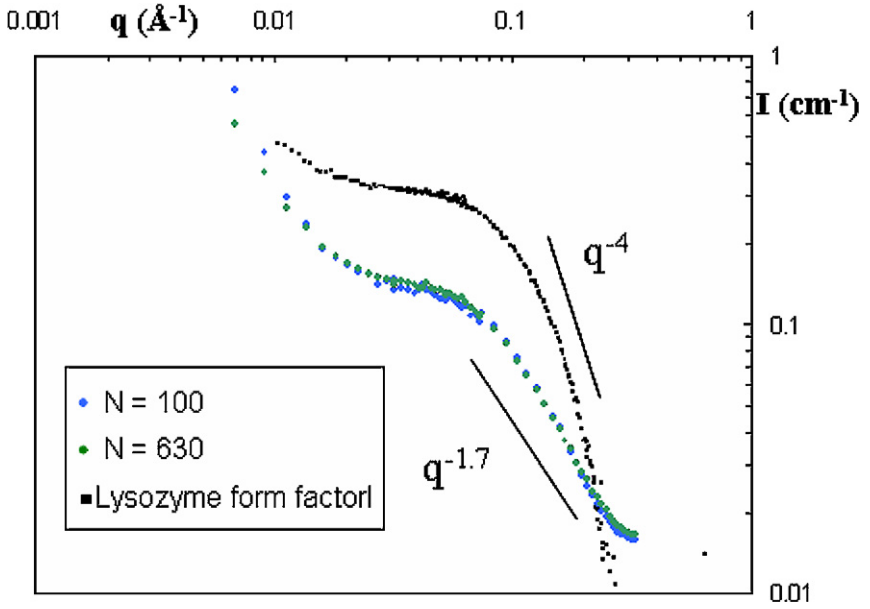

Fig. 3. Scattering signal of lysozyme—polymer is matched—within the complexes for $[-]/[+]_{\text{introduced}} = 20$ ([lysozyme] = 20 g/L; [PSSNa] = 0.3 mol/L). Black symbols: signal of lysozyme form factor (measured at 10 g/L and magnified here by a factor 4 instead of 2 in order to make curves distinguishable). Blue symbols: complexes made with small chains ($N = 100$). Green symbols: complexes made with chains of intermediate length ($N = 360$).

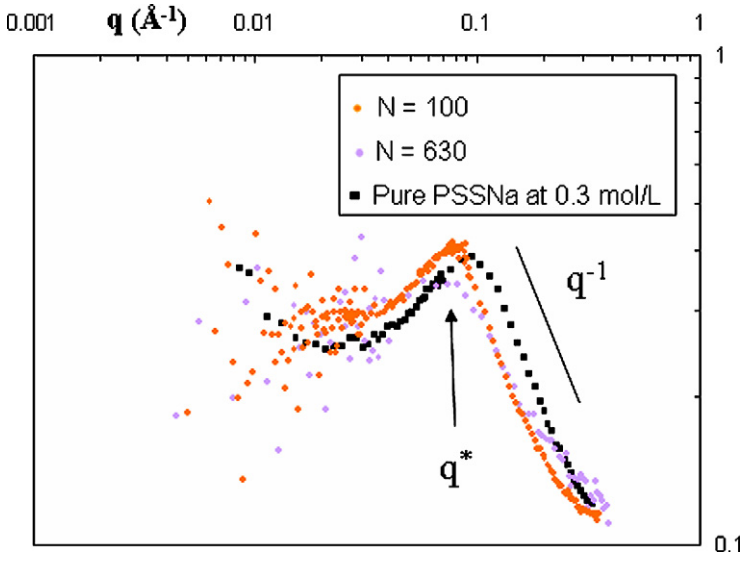

Fig. 4. Scattering signal of PSS chains within the complexes (lysozyme is matched) for $[-]/[+]_{\text{introduced}} = 20$ ([lysozyme] = 20 g/L; [PSSNa] = 0.3 mol/L) as for Fig. 3. Black symbols: signal of a pure solution of PSSNa at 0.3 mol/L. Orange symbols: complexes made with small chains ($N = 100$). Mauve symbols: complexes made with chains of intermediate length ($N = 360$). Full squares: complexes made with small chains ($N = 625$).

from a fractal object of dimension D_f: this is indeed the fractal dimension of a Self Avoiding Walk (while random walk has a fractal dimension $D_f = 2$). It has been shown formerly [12,13] that a $q^{-1.7}$ law is also obtained for an unfolded protein. So we can infer, from such a direct measurement, that the conformation of lysozyme inside the complexes has changed: the protein is no longer in its native state (this has been checked by spectroscopy).

In the same system, if now we match the protein signal, and look at the polyelectrolyte one in Fig. 4, the scattering shape is strongly different. At $q^* \approx 0.08$ Å^{-1}, we see a maximum characteristic of electrostatic repulsion between

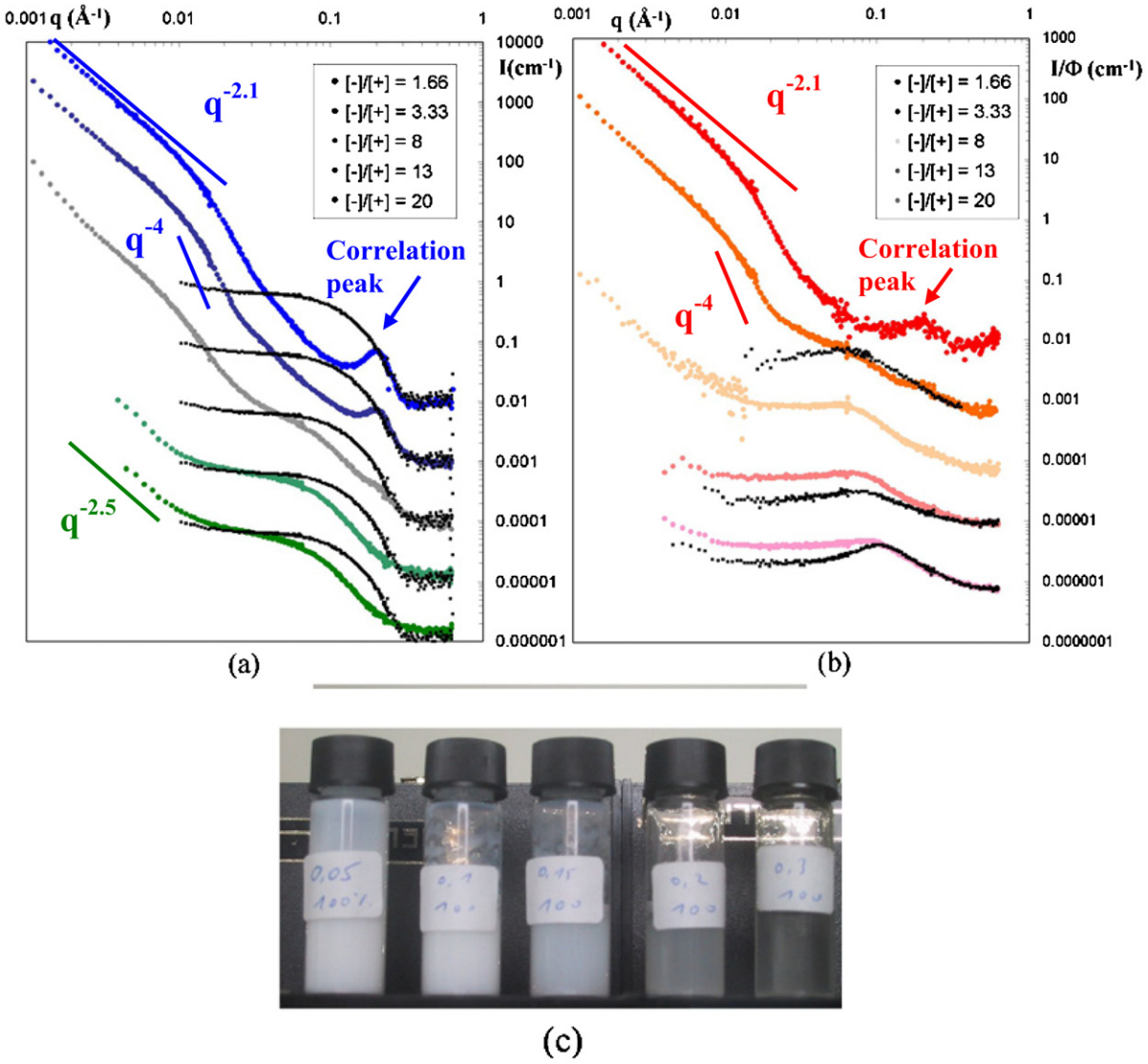

Fig. 5. SANS curves as a function of the introduced charge ratio: (a) scattering of lysozyme (40 g/L) for all 5 ratios $[-]/[+]_{\text{introduced}}$ noted $[-]/[+]$ in the figure. Each curve is shifted by a factor 10, and compared to that of diluted lysozyme (10 g/L) measured in same contrast conditions, multiplied by a factor 4, and plotted in black points. (b) Scattering of polyelectrolyte for the same five charge ratios (shifted each by 10), and compared to the one of pure PSS Na solutions measured in same contrast conditions and plotted in black points. (c) Macroscopic aspect of the five samples: from left to right, samples are less and less turbid when increasing $[-]/[+]_{\text{introduced}}$.

charged chains. At large q, PSS chains scatter as q^{-1}, as expected for one-dimensional rod-like objects ($D_f = 1$) with short scale rigid structure due to electrostatic repulsions. Both features are present in pure PSSNa solutions (continuous curve of Fig. 4).

In summary, we see distinctly the scattering of the two objects, although they are very different. Meanwhile, a small correlation between species is visible through a common feature of both spectra: at low q, in the signal of *lysozyme* in the complexes, a slight 'shoulder' can be seen at the same q^* as for the scattering of polyelectrolyte: this suggests that the networks formed by the two chain-like objects are interpenetrated. The protein is unfolded and simply coexists with the polyelectrolyte chain without larger spatial concentration fluctuations. This agrees with the fact that solutions are macroscopically clear in this regime.

Let us now consider in Fig. 5 the evolution of the mixture scattering with the quantity of polyelectrolyte chains added, measured in terms of the ratio of charges introduced, $[-]/[+]_{\text{introduced}}$. At large ratio (*lower curves*), we recover

the behavior just described. At a lower ratio, we know that the visual aspect of the samples shows a transition towards a second region of the phase diagram where samples become more and more turbid (see Fig. 5).

At the same time, the scattering (*upper curves*) shows a second type of complexation [4–6]. It displays very different features, which also make appear several different q ranges, detailed below:

- at *large* q, the scatterings from the two species are *different* from each other (as above). As in pure PSS solutions, the PSS signal is akin to that of a semi-flexible individual chain (which will be detailed below in Section 3.4): it approaches progressively the signal of a rod (q^{-1} as $D_f = 1$) at the largest q's. In this same large q range, the protein signal is also identical to that of an individual protein: it displays a q^{-4} law. But at intermediate q, a *new effect is visible*: a pronounced maximum can be seen at $q \sim 2\pi/R_{\text{lys}}$. This is characteristic of close contact between two proteins inside the complexes. We have thus again a quite accurate and independent description of the two species using these two different contrasts;
- at *low* q, *the situation is reversed*. Instead of being *different*, the signals of lysozyme (when PSS is matched) and of PSS (when lysozyme is matched) display an *identical* variation with q. Remember that we look at the *upper curves* in both left and right pictures. When going from large to low q, we first see an increase, corresponding to a q^{-4} law. This law, which is characteristic of compact objects with sharp interface as said above, is observed here again, but at much lower q range (hence much larger scale) than for the lysozyme protein q^{-4} law described above. Looking at a slightly lower q (still for *upper curves*), we see that the signal bends down and follows a rounded curve: this corresponds to the Guinier law for this compact globule, which we can call 'primary aggregate'. We can actually fit the signal in such Guinier range and in the q^{-4} regime to the scattering calculated for spherical 'globules' of radius R_{comp} of order 10 nm.

The fact that both species give the same signal in this q range means that both species are located in spherical globules. Before discussing this in detail, let us describe the last regime, observed at the lowest q available of upper curves: we see that a new power law $q^{-\alpha}$ is clearly present, with $\alpha = 2.1$. Here as before, the exponent for such a power law can be the fractal dimension of aggregates D_f. The value 2.1 can indeed be attributed to fractal aggregation of the primary aggregates (globules): it turns out that this is the one observed for reaction limited aggregation; here the limiting 'reaction' can be attraction between electrostatics species, as observed elsewhere. The $q^{-2.1}$ law is observed down to the lowest q: no Guinier regime is visible for these 'secondary' aggregates. Their size is larger than the accessible range.

4.2.1. Connection with real space and larger scales

Since, as we just discussed, the aggregates have larger sizes than those accessible by our measurements, we used real space imaging through electronic microscopy after cryofracture [7] in order to access larger scales. In Fig. 6, we can see grape-like aggregates which can be attributed to the fractal behaviour deduced from SANS. This is an example of the connection between observations in the q space and imaging in real space at larger scale. It is clear that no complete information can be gained from a single picture. The fractal behaviour is not seen clearly and necessitates interpretation. We can check that large aggregates are present, as suggested by SANS, but access to the maximum size of the largest aggregates would require examination of a much larger number of pictures. On the contrary, the *globule* size is well apparent. Correcting from the fact that the apparent size depends on the distance from the centre of the object to the fracture plan, we find largest sizes around 15–20 nm. One gets a visual insight of the narrow distribution. This agrees with the accurate values of radius R_{comp} (12 nm for lysozyme, 15 nm for PSS) and variance σ (0.37) obtained by SANS on the same sample.

4.2.2. Low q effective neutron contrast

In this specific scattering situation we can largely extend our analysis taking advantage of the identity of scattering length densities from both species [4,6]. We can assume that below 0.03 Å^{-1} the scattering is only due to the complexes. This allows us to introduce here the very classical formula for centrosymmetric objects in solution:

$$I_{\text{lyso}}(q)\ (\text{cm}^{-1}) = \Phi_{\text{comp}} \Delta\rho^2_{\text{comp}} V_{\text{comp}} P_{\text{comp}}(q) S_{\text{comp}}(q) \quad \text{for } q < 0.03\ \text{Å}^{-1} \tag{11}$$

where Φ_{comp} is the volume fraction of the complexes, V_{comp} is their volume, $\Delta\rho^2_{\text{comp}}$ the effective neutronic contrast between the complexes and the solvent, P_{comp} their form factor and S_{comp} their structure factor.

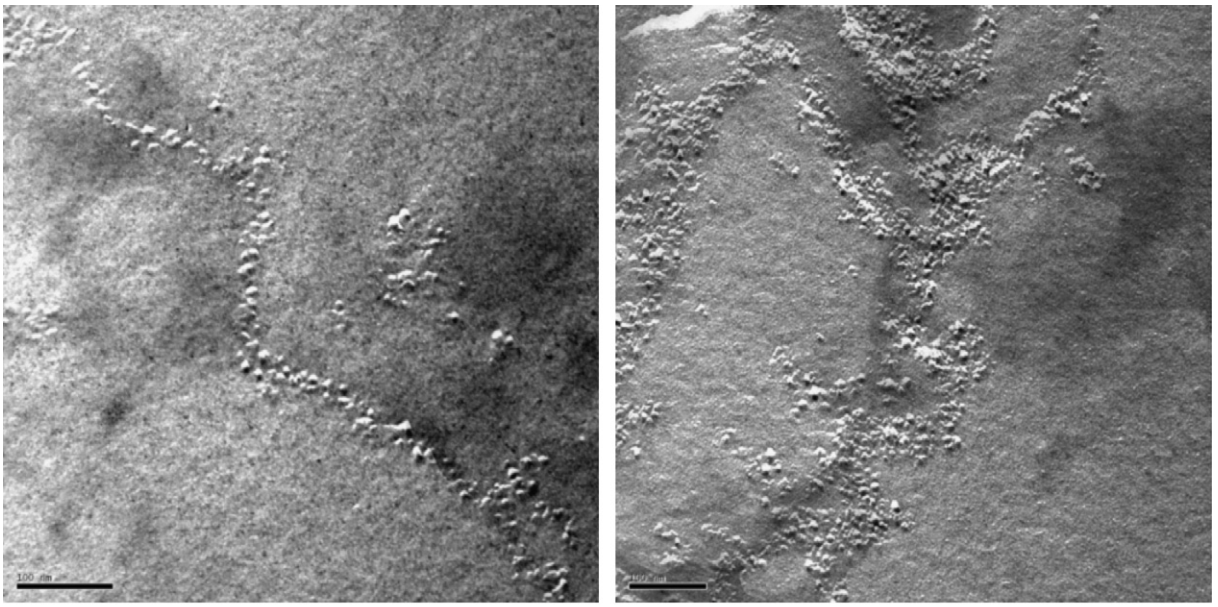

Fig. 6. Transmission Electronic Microscopy pictures after cryofracture for sample with introduced charge ratio $[-]/[+]_{\text{introduced}} = 1.6$. Square edge of the picture ∼0.5 μm.

Let us focus more on the term $\Delta\rho^2_{\text{comp}}$, which is the key point of our analysis. It is an effective neutronic contrast, i.e. the difference between the scattering length density of the solvent ρ_{solvent}, and an average scattering length density of the complex ρ_{comp}, *since the latter can be considered as homogeneous on the scale of observation*. Let us take the case where the polyelectrolyte is matched, and the lysozyme visible. The average composition of the complex comprises lysozyme with an inner volume fraction $\Phi_{\text{lyso\_inner}}$, and the solvent and polyelectrolyte chains, which occupy together a volume fraction $(1 - \Phi_{\text{lyso\_inner}})$ and have here the same scattering length density as the solvent, ρ_{solvent}. So we can write:

$$\rho_{\text{comp}} = \Phi_{\text{lyso\_inner}}\rho_{\text{lyso}} + (1 - \Phi_{\text{lyso\_inner}})\rho_{\text{solvent}} \tag{12}$$

and the effective contrast between the complex and the solvent becomes a very simple expression:

$$\Delta\rho^2_{\text{comp}} = (\rho_{\text{comp}} - \rho_{\text{solvent}})^2 = \Phi^2_{\text{lyso\_inner}}(\rho_{\text{lyso}} - \rho_{\text{solvent}})^2 = \Phi^2_{\text{lyso\_inner}}\Delta\rho^2_{\text{lyso}} \tag{13}$$

This makes two things possible.

First, if we fit the scattering, in the region where $S_{\text{comp}}(q) = 1$ (this is when $q > 1/R_{\text{comp}}$), to the form factor of a sphere (a very classical expression), of radius R_{comp} and volume V_{comp}, the front factor will give us the apparent contrast $\Delta\rho^2_{\text{comp}}$, and from it we get $\Phi^2_{\text{lyso\_inner}}$ the squared inner lysozyme fraction.

Second, we know that the same equation is valid for PSS when lysozyme is matched, replacing 'lyso' by 'PSS' in the indices above. Hence this prompts us to look at the ratio $I_{\text{lyso}}(q)/I_{\text{PSS}}(q)$ between the two signals: if the variations are similar, this ratio is constant with q and exactly equal to $\Phi^2_{\text{lyso\_inner}}/\Phi^2_{\text{PSS\_inner}}$! This is particularly exciting in the example given here, since we are interested in the inner charge ratio of the electrostatic complexes, $[-]/[+]_{\text{inner}}$. We see on Fig. 7 two different cases:

(i) for ratio $[-]/[+]_{\text{introduced}} \leqslant 1$ (values 0.65 and 1), the ratio $I_{\text{lyso}}(q)/I_{\text{PSS}}(q)$ is indeed constant (lower curves of Fig. 7). Moreover, its value, when correcting by the different factors, yields $[+]/[-]_{\text{inner}} = 1$;

(ii) for $[-]/[+]_{\text{introduced}} > 1$ (values 1.66 and 3.33, upper curves), i.e. a larger amount of polyelectrolyte, the ratio $I_{\text{lyso}}(q)/I_{\text{PSS}}(q)$ is not perfectly constant: it is decreasing at low q. This means that the polyelectrolyte scattering decreases faster with q, i.e. that the sphere occupied by the polyelectrolyte is larger than that of the protein. This

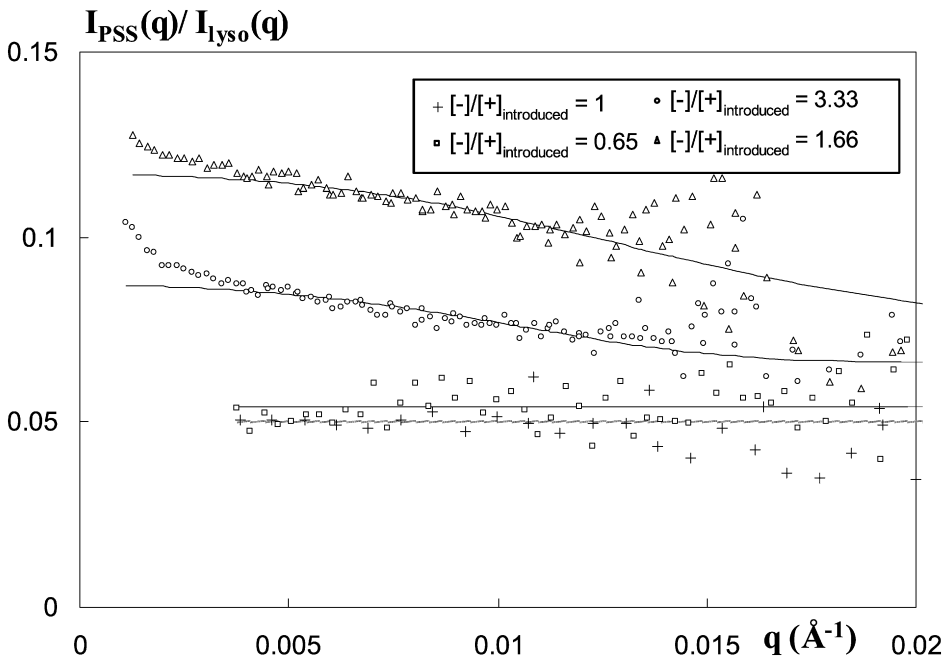

Fig. 7. $I_{PSS}(q)/I_{lyso}(q)$ at low q. Open circles: $[-]/[+]_{introduced} = 3.33$; open triangles: $[-]/[+]_{introduced} = 1.66$; crosses: $[-]/[+]_{introduced} = 1$; open squares: $[-]/[+]_{introduced} = 0.65$. The continuous lines correspond to the fits of sphere and sphere plus corona scattering (see Ref. [6]) for $[-]/[+]_{introduced} = 3.33$ and $[-]/[+]_{introduced} = 1.66$. The dashed line ordinate is 0.055. The dotted line ordinate is equal to 0.05.

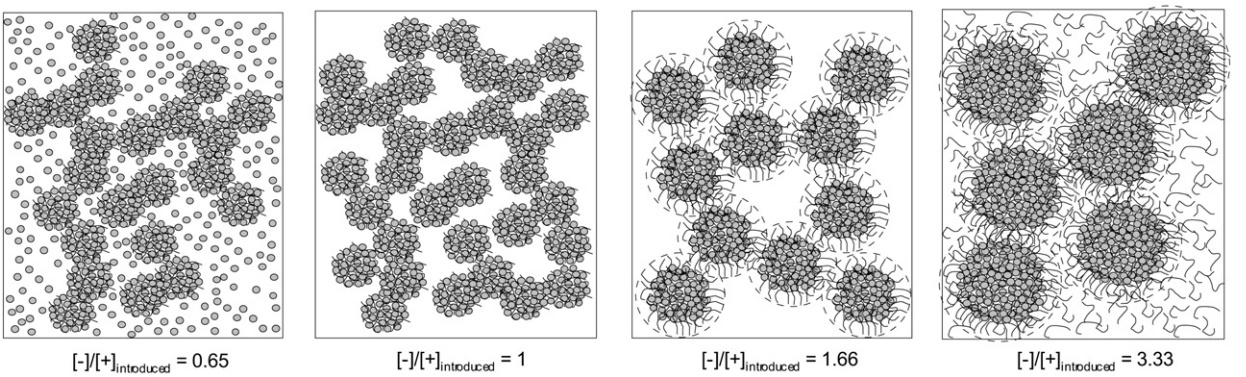

Fig. 8. Pictures of the different structures of lysozyme–PSSNa complexes as suggested by SANS when $[-]/[+]_{introduced}$ is "close to 1" (here in between 0.65 and 3.33).

can be explained by the presence of a polymer corona around a compact core of polymer plus protein. This picture agrees with the extra negative charge observed in this regime.

These analyses are translated into real space in Fig. 8, which shows pictures of the different structures of lysozyme–PSSNa complexes around $[-]/[+]_{introduced} = 1$.

4.2.3. Kinetic evolution of samples after synthesis

Like X-ray or light scattering, neutron scattering allows one to follow a kinetic evolution. To illustrate this, we keep our lysozyme–PSS system. We have studied, in the early stages after its realization, one sample with a high polymer ratio, $[-]/[+]_{introduced} = 20$, which, after a long time, eventually evolves to completely unfolded protein and weak scattering at small q. Fig. 9 presents the results recorded in the first hour from 2 min (upper log–log curves) to 60 min. We see in the log–log plot a rapid vanishing with time of the low q signal: we learn that the globules

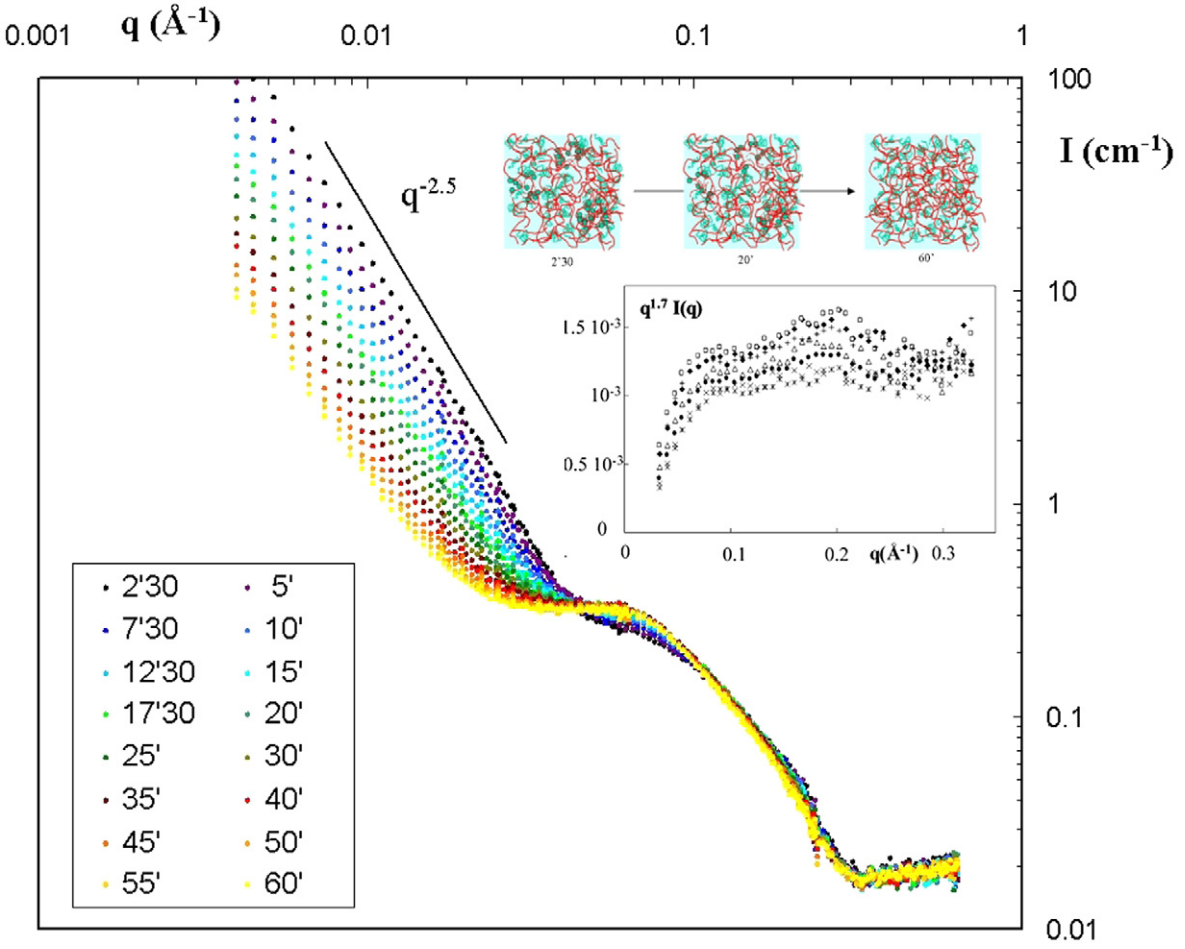

Fig. 9. Early stages of kinetics (from 2 min 30 sec to 60 min), for the protein signal (polymer is matched) in a lysozyme–PSS mixture with large excess of polymer: $[-]/[+]_{\text{introduced}} = 10$ ([lysozyme] = 40 g/L; [PSSNa] = 0.3 mol/L). Insert: a $I(q)q^{1.7} = f(q)$ representation, showing the fractal behavior and the vanishing of the medium q maximum due to correlations between proteins inside the aggregates, for a similar kinetics (successive frames of 10 min each) at same concentrations.

are first immediately formed, and progressively redissolved. Let us then focus on the insert plots, which represent $q^{D_f} \cdot I(q)$ versus q in a similar kinetics study. Such a plot is widely used for showing a q^{-D_f} law, in particular for large q behaviours, since it is much more sensitive. Here $D_f = 1.7$, and we observe that at the beginning (upper curves of the insert) there is an oscillation corresponding to the maximum for proteins at contact; this oscillation vanishes progressively with time, simultaneously with the disappearance of the low q globules scattering.

4.3. Matching several species in a multiple system: example of counterions localisation in polyelectrolyte–protein complexes

We will now consider here a quaternary system, in which we will match two species to the solvent. We are then able to observe distinctly the fourth one. We keep as an example our PSS–lysozyme system, where we can use the rare and invaluable advantage that hydrogenated PSS chains and lysozyme have exactly the same scattering length density ρ. Thus the scattering from both species can be switched off simultaneously (by a 57%H_2O/43%D_2O solvent mixture). We can see the fourth component, which is the counterions, if we can make their ρ different enough, using labelling. This is possible [4,8] by replacing the Na^+ counterions by deuterated TetraMethylAmmonium d-TMA^+ counterions, which have the same valence, and are known to behave similarly (contrary to what the chemical formula crudely suggests). The signal is the scattering of the deuterated counterions only, and we can check whether they are released

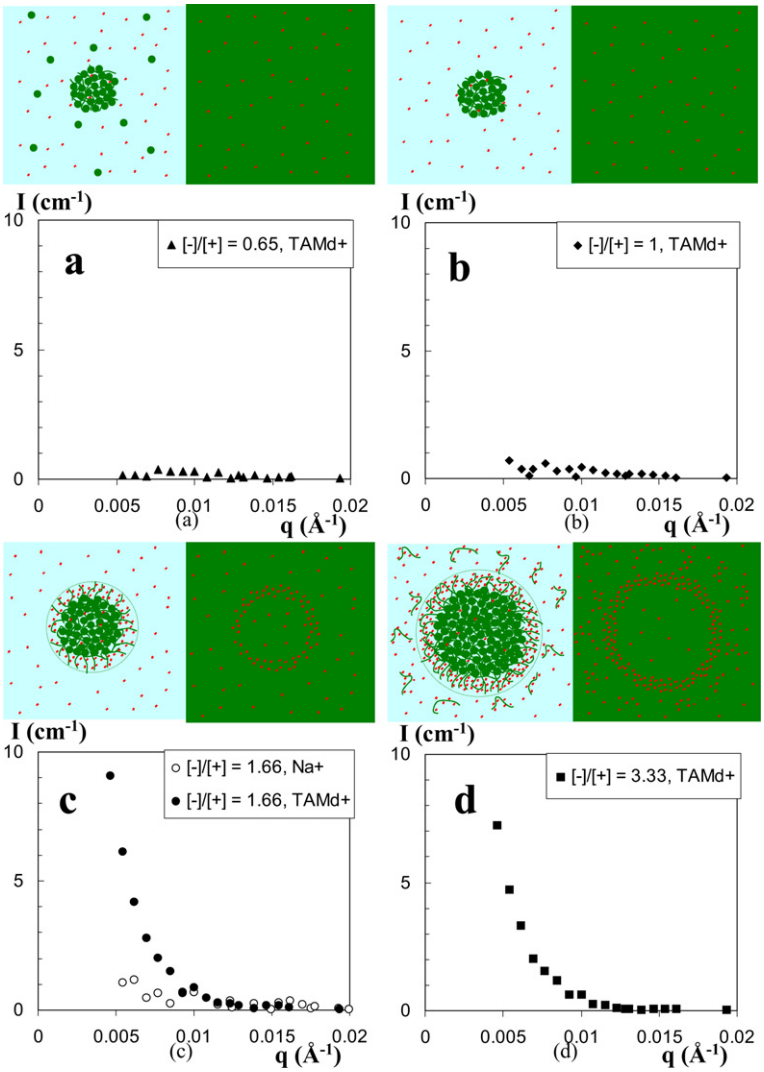

Fig. 10. Pictures: Structures of globules made of lysozyme (green), h-PSS (green), and $(CD_3)_4N^+$ counterions (red) in 100% H_2O solvent (left, light blue background) or in 57%H_2O/43%D_2O solvent (right, green background). Curves: corresponding scattering of $(CD_3)_4N^+$ in the 57%H_2O/43%D_2O solvent. (a) and (b): 'naked cores' ($[-]/[+]_{introduced} = 0.65$ and $[-]/[+]_{introduced} = 1$). (c) and (d): 'hairy cores' ($[-]/[+]_{introduced} = 1.66$ and $[-]/[+]_{introduced} = 3.33$). On the lower left-hand side figure, is also plotted the scattering in 57%H_2O/43%D_2O with Na^+ c.i. which shows very low compared to that with $(CD_3)_4N^+$ c.i.

in the solvent or gathered around the globule. We get a 'yes or no' check, unambiguously linked to the presence or not of the chain counterions in protein–polyelectrolyte complexes by choosing 4 samples which should, or should not, have released only counterions, and hence who should scatter, or not. These four samples, which correspond to the four typical structures described above in Fig. 8, are illustrated with respect to the localisation of counterions in Fig. 10. In short, by varying $[-]/[+]_{intro}$ we can pass from 'naked' cores, where all c.i. (counterions) should be released, to 'hairy' cores, where some c.i. are still present because they are condensed on the dangling polyions of the shell. In order to do this experiment, we first check the effect of TMA on the globule size using non-deuterated TMA counterions which are matched by H_2O-rich solvent, with deuterated PSS polyelectrolyte. Then we replace d-PSS by normal PSS, and TMA by d-TMA.

On Fig. 10, at first sight, samples containing 'naked' globules ($[-]/[+]_{intro} = 1$ and 0.65) *do not scatter* at low q, while samples with 'hairy' globules ($[-]/[+]_{intro} = 1.66$ and $[-]/[+]_{intro} = 3.33$) *do scatter*. A control sample with Na^+ counterions has been measured for $[-]/[+]_{intro} = 1.66$. Compared with the d-TMA scattering in Fig. 10, its

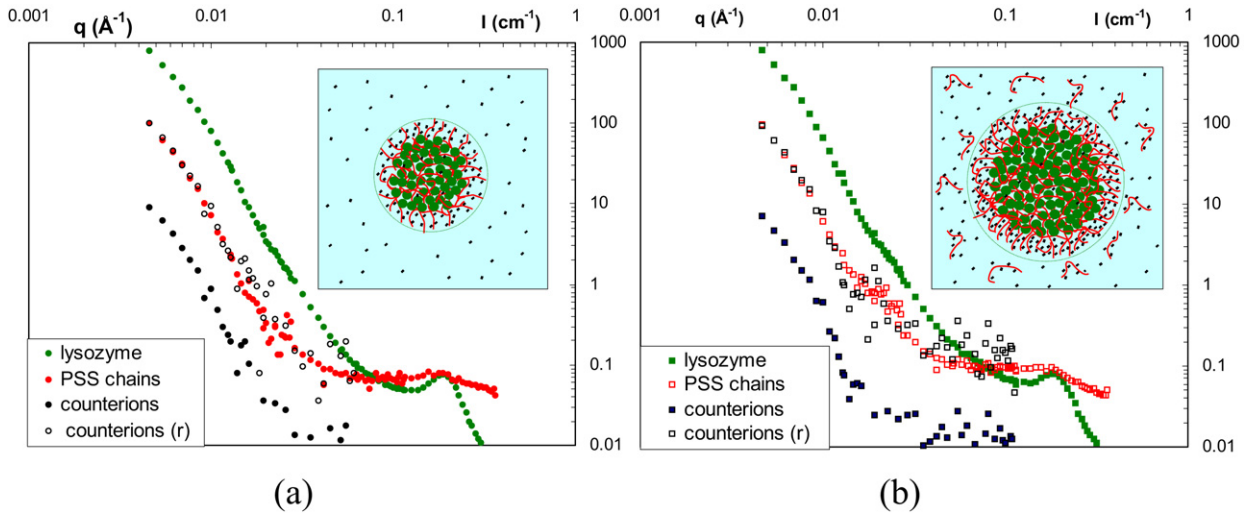

Fig. 11. Counterions release: (a) $[-]/[+]_{\text{introduced}} = 1.66$; (b) $[-]/[+]_{\text{introduced}} = 3.33$. Full squares: lysozyme scattering (in 100%D_2O solvent). Red crosses: PSS scattering (d-PSS in 57%H_2O/43%D_2O solvent). Black crosses: c.i. $(CD_3)_4N^+$ (in 57%H_2O/43%D_2O solvent with h-PSS chains) in hairy globules. Open symbols: c.i. scattering renormalized—noted counterions(r) in the figure caption, in order to facilitate comparison with the signal from d-PSS.

scattering at low q is very small. This confirms that the low q scattering from hairy globules comes from the d-TMA counterions.

In order to check whether this scattering comes from the decoration of the shell by the counterions, we compare it to the d-PSS chains scattering. They should be proportional to each other. The ratio, which we will call F, is the square of a product of two terms:

- the ratio of the d-TMA and d-PSS contrasts, which is close to 1, because the neutron density length of $(CD_3)_4N^+$ and d-PSS are close;
- the ratio of the d-TMA c.i. and d-PSS volume fractions, equal to $(1 - f).V_{\text{c.i.}}/V_{\text{PSS}}$, where f is the fraction of free counterions equal in Manning's condensation theory to 0.66 for PSS Na. Applying this value, together with our estimate of $V_{\text{c.i.}}/V_{\text{PSS}}$, we obtain a value of F not very far from the experimental value found equal to 10. This is a good support of the picture of decoration of the PSS shell by counterions which we proposed.

In summary, contrast matching has allowed us to show that when no polymer corona is present, there are no counterions around the spheres, and hence counterions are released in the solvent, which gives an entropy gain to the system.

4.4. Zero deuterated fraction extrapolation for chain form factor in polyelectrolyte–protein complexes

Using for the third and last time the example of polyelectrolyte–protein complexes, we show how to extrapolate the contribution from scatterers belonging to the same individual object, here a chain, in the case where such objects have strong intercorrelations due to interdispersion—we could say 'interminglement' for chains—among the mixed system [9]. The q dependence of this intrachain contribution is accounted for in the so-called form factor (normalised to 1 at zero q limit). This section will be an opportunity of introducing the form factor of a polymer chain.

The system is equivalent to a quaternary system: protein (1), non-deuterated h-PSS (2), solvent (3), and a fraction of deuterated PSS (4). Because h-PSS and protein have very close scattering length densities, we can match them both by the same 57%H_2O/43%D_2O mixture (as just above in Section 3.3). So deuterated d-PSS is the only visible species. To get the single chain contribution, we can then extrapolate the d-PSS signal to zero d-PSS concentration. Of course, this makes sense only if the total PSS concentration ($c_{\text{d-PSS}} + c_{\text{h-PSS}}$) is kept constant.

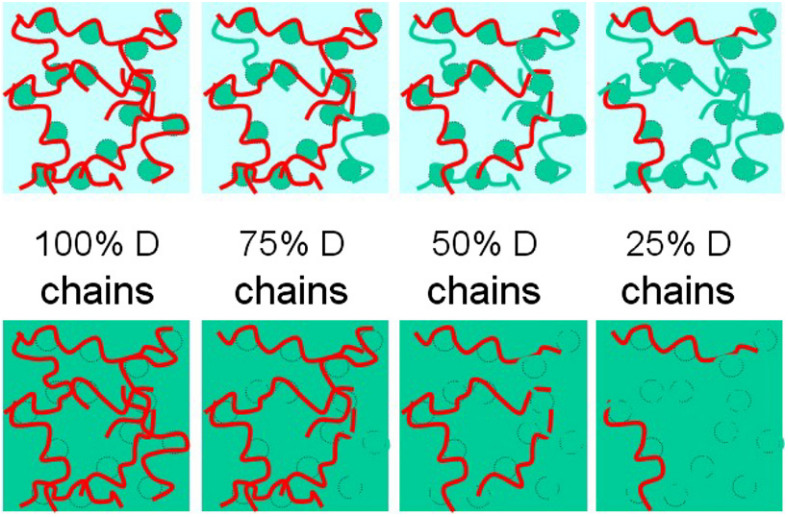

Fig. 12. Sketch figuring the extrapolation of the single chain scattering.

This is schematized in Fig. 12. Because we match h-PSS, only the $S_{\mathrm{DD}}(q)$ term is present and:

$$I(q)\ (\mathrm{cm}^{-1}) = K_{\mathrm{D}}^2 V_{\mathrm{mol}}^2 \left\{ \Phi_{\mathrm{D}} S_{1\mathrm{D}}(q) + \Phi_{\mathrm{D}}^2 S_{2\mathrm{D}}(q) \right\} \tag{14}$$

where K_{D}^2 is the contrast between d-PSS chains and the solvent, and V_{mol} the molecular volume of one chain unit. $S_{1\mathrm{D}}(q)$ is the scattering from couples of segments from the same d-chain, and $S_{2\mathrm{D}}(q)$ from two different d-chains (we use for h-chains the same notations for $S_{1\mathrm{H}}$, $S_{2\mathrm{H}}$, with H instead of D, and $S_{2\mathrm{HD}}(q)$ between one d-chain and one h-chain). Since the total concentration is constant and all chains are identical apart from deuteration, $S_{1\mathrm{D}}(q)$ $(=S_{1\mathrm{H}}(q))$ can be noted $S_1(q)$ $(\mathrm{Å}^{-3})$, and $S_{2\mathrm{D}}(q)$ $(=S_{2\mathrm{H}}(q) = S_{2\mathrm{HD}}(q))$ noted $S_2(q)$ $(\mathrm{Å}^{-3})$. Finally,

$$I(q)\ (\mathrm{cm}^{-1})/(K_{\mathrm{D}}^2.V_{\mathrm{mol}}^2 \Phi_{\mathrm{D}}) = S_1(q) + \Phi_{\mathrm{D}} S_2(q) \tag{15}$$

We will measure solutions with four values of Φ_{D} at constant total concentration of chains; for each q value we will get a series of four intensities. By extrapolation of $I(q)/\Phi_{\mathrm{D}}$ to $\Phi_{\mathrm{D}} = 0$, we get the value of $S_1(q)$ at this q value.

To check the validity of this zero Φ_{D} extrapolation, we applied it first to a pure PSS solution. Doing this we repeat an experiment done some years ago in the Polymer Group at Saclay [14] ($S_1(q)$ was later obtained by an even more direct method, called Zero Average Contrast (ZAC), detailed in Appendix A).

In order to discuss the three form factors obtained, we recall now in more detail the q dependence in usual polyelectrolyte solutions:

(1) at $q < 1/R_g$, the complete intrachain scattering $S_1(\mathbf{q})$ tends at $q \to 0$ towards:
$S_1(q \to 0)\ (\mathrm{Å}^{-3}) = (1/V_{\mathrm{mol}}).N_w.P(\mathbf{q})$, where N_w is the weight average of the number of units in one chain. We have $\lim_{q\to 0}(P(q)) = 1$, and all the q dependence is contained in $P(q)$, which can be written at low q (see Eq. (10)): $P(q) \sim 1 - q^2 R_g^2/3$, R_g being the radius of gyration of the chain;

(2) in the so-called 'intermediate' range, $q > 1/R_g$, $P(q)$ gives information from the inside of the object. For a wormlike chain, one has two ranges:
- at sizes $\mathbf{r}$ larger than the persistence length l_p, for $q < 1/l_p$, the conformation is that of a Gaussian chain, a random walk. Since the fractal dimension of a random walk is 2, $S_1(q)$ and $P(q)$ vary as $1/q^2$;
- at distances smaller and smaller than l_p, the chain appears more and more rigid. The curve followed by the chain in real space is such that if Ψ is the angle between the tangents of two points of the chains separated by a curvilinear distance l, then:

$$\langle \cos \Psi \rangle \approx \exp(-l/l_p) \tag{16}$$

- at larger q, the chain is rigid, so the fractal dimension is $D_f = 1$, and $S_1(q) \sim q^{-1}$.

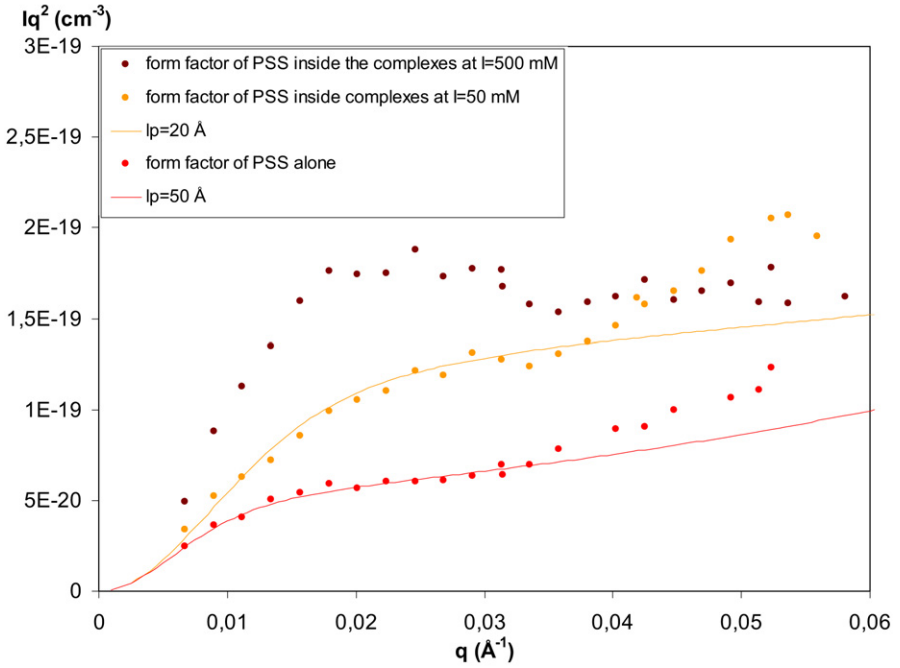

Fig. 13. 'Kratky plot' ($q^2 I(q)$ vs q) of the three I/Φ_D signals extrapolated at zero deuterated volume fraction Φ_D, proportional to the chains form factors for PSS: alone (lower curves, red dots), inside the gel structure (middle curve, yellow dots) and inside the globular structure (upper curve, brown dots) as well as the three corresponding fits (solid lines).

To visualize better the signal of the form factor, a convenient representation is the Kratky plot, $q^2.I(q) = f(q)$, represented in Fig. 13, from $q = 10^{-3}$ to $q = 6 \times 10^{-2}$ with a linear q axis. This allows careful comparisons with calculations in the frame of the wormlike chain model [15]. At low q, $S_1(q)$ tends to a constant, so $q^2 I(q)$ is null at $q = 0$. For $q.l_P < 4$, Sharp and Bloomfield [16a] give the following expression:

$$P(q) = \frac{2(\exp(-x) + x - 1)}{x^2} + \left[\frac{4}{15} + \frac{7}{15x} - \left(\frac{11}{15} + \frac{7}{15x}\right)\exp(-x)\right]\frac{2l_p}{L} \tag{17}$$

with $x = Lq^2 l_p/3$, L being the chain length. This describes both the Guinier range, where $q^2 I(q)$ is increasing, and the Gaussian chain spatial range, where $q^2 I(q)$ displays a plateau, since $I(q) \sim q^{-2}$. When $q.l_p > 4$, the signal follows the asymptotic law of des Cloizeaux [16b]:

$$P(q) = \frac{\pi}{qL} + \frac{2}{3q^2 L l_p} \tag{18}$$

for which the quantity $q^2.I(q) \sim q^2.q^{-1} \sim q$ is increasing again. We show the result of a fit (L being known, the fitting parameter is l_p) on Fig. 13. For pure PSS, the best fit is for $l_p = 50$ Å. This is the value given in the literature for the same ionic strength as in our solutions (0.05 M buffer, $c_{PSS} = 0.1$ M). It is a combination of the intrinsic persistence length l_0 due to the chemical rigidity chains (∼10 Å) with the electrostatic persistence length l_e due to the repulsion between the charged monomers.

The extrapolated signal for PSS inside the gel structure is represented on Fig. 13 in the Kratky plot and compared with the signal of the PSS chains alone in solution. A change in the persistence length of the chains can be seen in two ways:

- the upturn position is at $q = 0.025$ Å^{-1} for the PSS inside the complexes when it is at $q = 0.015$ Å^{-1} for the PSS alone;
- the plateau value is 5×10^{-20} cm^{-3} for the PSS alone, when it is 12×10^{-20} cm^{-3} for the PSS inside the complexes.

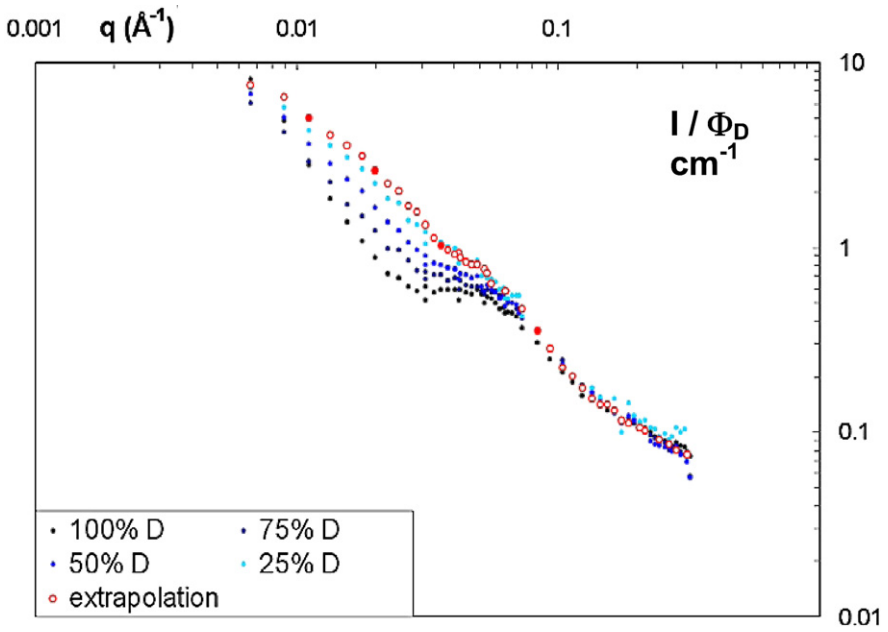

Fig. 14. Scattering cross-section I (cm^{-1}) normalized to deuterated chain volume fraction (I/Φ_{D}), and zero Φ_{D} extrapolation, proportional to the form factor of PSS chains in complexes.

Since the plateau height varies as $1/l_p$, the persistence length has undoubtedly decreased; the fit gives a best value $l_p = 20$ Å instead of 50 Å for the PSS alone.

In summary, after interaction with the protein, in the gel phase, the PSS chains are shrunk. Note that these changes in $S_1(q)$ are accompanied by corresponding changes in the scattering for $\Phi_{\mathrm{D}} = 1$. We can see in Fig. 5 that the position of the 'polyelectrolyte peak', is shifted towards lower values of q: the chains being shrunk, they are further apart.

Finally, let us look at the conformation of the PSS chains inside the globular complexes. To be consistent we wished to use the same chains. Hence, in order to obtain a transition towards the globule regime, we used another parameter affecting the transition, the ionic strength, which we increased to 0.5 M. Of course, we first have used the 100% deuterated sample to check this globular structure. Before looking at the Kratky plot of extrapolated data, let us look for this sample at the extrapolated signal in log I versus log q representation. On Fig. 14 are represented the four PSS signals (in $I(q)/\phi_{\mathrm{D}}$) for $\Phi_{\mathrm{D}} = 100\%$, 75%, 50% and 25%, as well as their extrapolation at $\phi_{\mathrm{D}} \to 0$:

- at low q, the PSS "total scattering" ($\Phi_{\mathrm{D}} = 100\%$) *increases* when $q \to 0$. Then, *when decreasing* Φ_{D}, this low q intensity *decreases*. This is opposite to the pure solution and gel case (curves not shown here), where the total scattering displayed a maximum, so that when *reducing the interchain* contribution at lower Φ_{D}, the intensity was *increasing* at low q;
- at the high q values, the inter-chains correlation peak imposed between chains by the inter-proteins contact correlations, vanishes as the deuteration ratio tends to zero, as expected. Thus, finally, the extrapolated signal seems not so different from the signals of pure PSS and PSS inside the gel structure; the high q region scatters like q^{-1} and crosses-over when decreasing q.

This last result is also represented in the $q^2 I$ representation on Fig. 13. It is possible to see immediately that the structure adopted by the PSS chains inside the dense complexes is completely different from that of the pure PSS chains in solution and inside the gel structure. The conformation adopted is no longer a wormlike chain. In the present case an apparent plateau can be seen. It can be attributed to a scattering like q^{-2}, which suggests that the chains are close to a Gaussian behaviour and behave as random walks inside the globules. Alternately, we can focus on the slight maximum observed in the $q^2 I$ plot. This can be attributed to a collapsed conformation, as observed at shorter scale in partially sulfonated PSS, which adopts a pearl necklace-like conformation [17].

4.5. Summary

In summary, using various possibilities of contrast matching in a polymer–protein complex, we have been able to measure separately the protein and the polymer signals. In the case where the structure was as simple as mixed globules, the contributions of the two species are proportional, so we can 'titrate' them *inside the globules.* Moreover, because the scattering length density of lysozyme was *equal* to that of the polymer (a very special case), we have also been able to measure the counterions signal, *and* the polymer form factor inside the globules. In the more general case when the scattering length densities are different, other possibilities can be explored, such as ZAC (see Appendix A).

5. Accuracy, absolute units and modelization

We will briefly discuss how neutron scattering allows us, through accurate measurements in absolute units, to compare data with theoretical models and calculations, analytical or from simulation.

5.1. Accuracy, absolute units

As discussed above, one advantage of neutrons for Small Angle Scattering is the high contrast available, in particular in the case of deuterium labelling. Hence a high enough scattering can be obtained, even if the incoming flux is weak. The collateral interesting aspect of low flux is that *all parasitic signals* such as scattering and reflexion by the collimation slits, as well as from sample container (which, moreover, is often the lowest in the case of neutrons compared to other radiations), or impurities in the sample *are low also and easy to correct*. The signal can be expressed in absolute cm^{-1} units, after normalisation by the water scattering, the cross-section of which can be measured on each spectrometer, in the corresponding conditions. Other advantages are:

- the sample is not damaged during the measurement, so the scattering does not evolve during the recording;
- multiple scattering is also often negligible, and the density of scattering length is well defined for each species, so that the contrast is well known.

Thus, finally, we obtain an accurate reproducible expression of the Fourier transform of the spatial correlations in absolute units.

5.2. The direct link between scattering and theory or simulation

Absolute units and measurement accuracy have a direct consequence: a quantitative comparison with theories. In soft matter, many calculations use analytical derivations in which the correlations are the key to the statistical calculation since entropy as well as the interaction spatial potential are often involved. In many cases, calculations are easier in Fourier space, giving directly such a result with a physical meaning. Computer simulations also are possible in Fourier space since the positions of the molecules are known, and thus the Fourier transform can be achieved during the computer calculation, and stored by authors allowing later comparisons with data.

For computer simulations, in the case of the polyelectrolyte complexes described above, extensive Monte Carlo calculations were performed [18]. To be brief, some of the results predict gel or globules and allow direct comparisons.

As we have seen, models for analytical calculation of the scattering were used to fit data on polyelectrolyte–protein complexes showed above: from simple one (sphere), to more complex one (semiflexible chain). In the next paragraph, we choose to present as an example, a slightly more complex calculation—namely, implying anisotropic chain scattering, in order to discuss the feasibility aspect of comparison with an experiment.

5.3. Silica particles and polymer in a deformed nanocomposite: observation of anisotropic scattering and proposal for modeling

We give here another brief example of mixed system implying polymer chains, which is often called a nanocomposite. It is a mixture of silica nanoparticles—first species—with chains of a film made of polymer—second species. In order to improve the mechanical reinforcement, we were interested in a better dispersion of the silica inside the

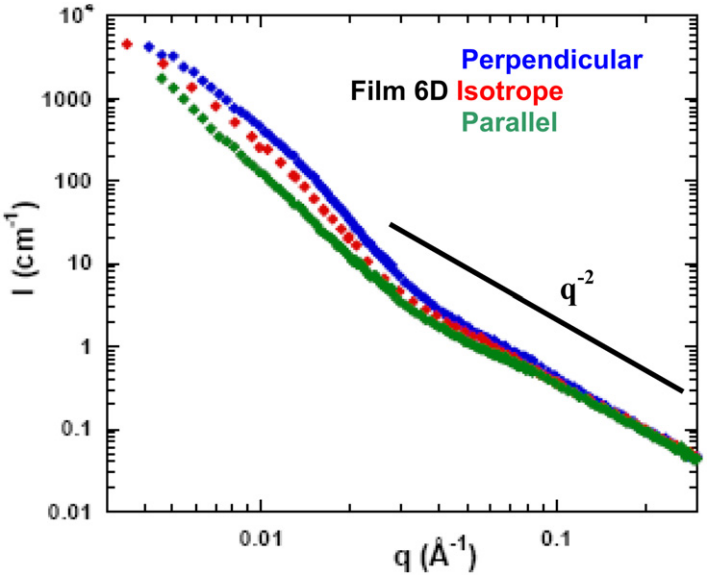

Fig. 15. Log–log representation of the measured scattering of films containing nanoparticles with hard silica core surrounded by polystyrene non-deuterated grafted chains in a deuterated PS matrix at rest before deformation (middle curve, red dots), and submitted to a macroscopic stretching of ratio $\lambda = \text{Length}/\text{Length}_{\text{initial}} = 2$. Upper curve (blue dots), scattering perpendicular to stretching axis. Lower curve (green dots), scattering parallel to stretching axis.

polymer matrix. In this aim we undertook the task of growing polymer chains from the surface of the silica particles [19–21]. Usually these chains are made of a non-deuterated polymer; if we disperse the particles in a deuterated matrix of the same polymer, there is a strong scattering contrast between the chains brought together with the silica particles and the matrix deuterated chains.

Indeed, looking at the red dots (which correspond to the scattering at rest, i.e. before deformation) in Fig. 15 [19] we observe a signal characterized by:

- at low q, a steep decrease, followed by a more 'rounded' part. In this q range we see both the scattering from polymer chains and the scattering of the silica core, which here has also a (smaller) contrast with the polymer matrix;
- at larger q, by a slower decrease with a q^{-2} variation. As explained above in Section 4.4, a q^{-2} law is characteristic of a Gaussian chain. This means that the deuterated chains brought together with the silica are interdispersed with the matrix non-deuterated chains. At the local scale, the system is akin to a mixture of D and non-D chains in a polymer melt. Such a mixture scatters neutrons, so the D chains are visualized. This signal dominates the silica contribution, which decays much faster (q^{-4} law).

Note at this stage that some other synthesis gave non-aggregated particles after purification. They were studied in solution, using contrast matching. We could see either the silica or the polymer, and fit the data to a well-defined core–corona object in this case [21].

In a second step, the nanocomposite films have been deformed (at a temperature $T = 112\,^{\circ}\text{C}$, about 30 °C above the glass transition, with a velocity gradient 0.007 s^{-1}). It is then possible to observe the deformation of the polymer shell within the sample. It is important to understand this particular interfacial region which is expected to be linked with the mechanical reinforcement. Indeed, the latter is much stronger than expected from simple hydrodynamics of hard spheres inside a fluid, as soon as the filler volume fraction becomes larger than a few percent; moreover, even if percolation concepts—introducing connections between the hard objects—are considered, connections seem to occur surprisingly below the expected volume fraction threshold. This suggests that the polymer at the surface of the fillers has a specific behavior. In Fig. 16 we observe on a X,Y multidetector at different sample–detector distances (shorter distances correspond to larger q):

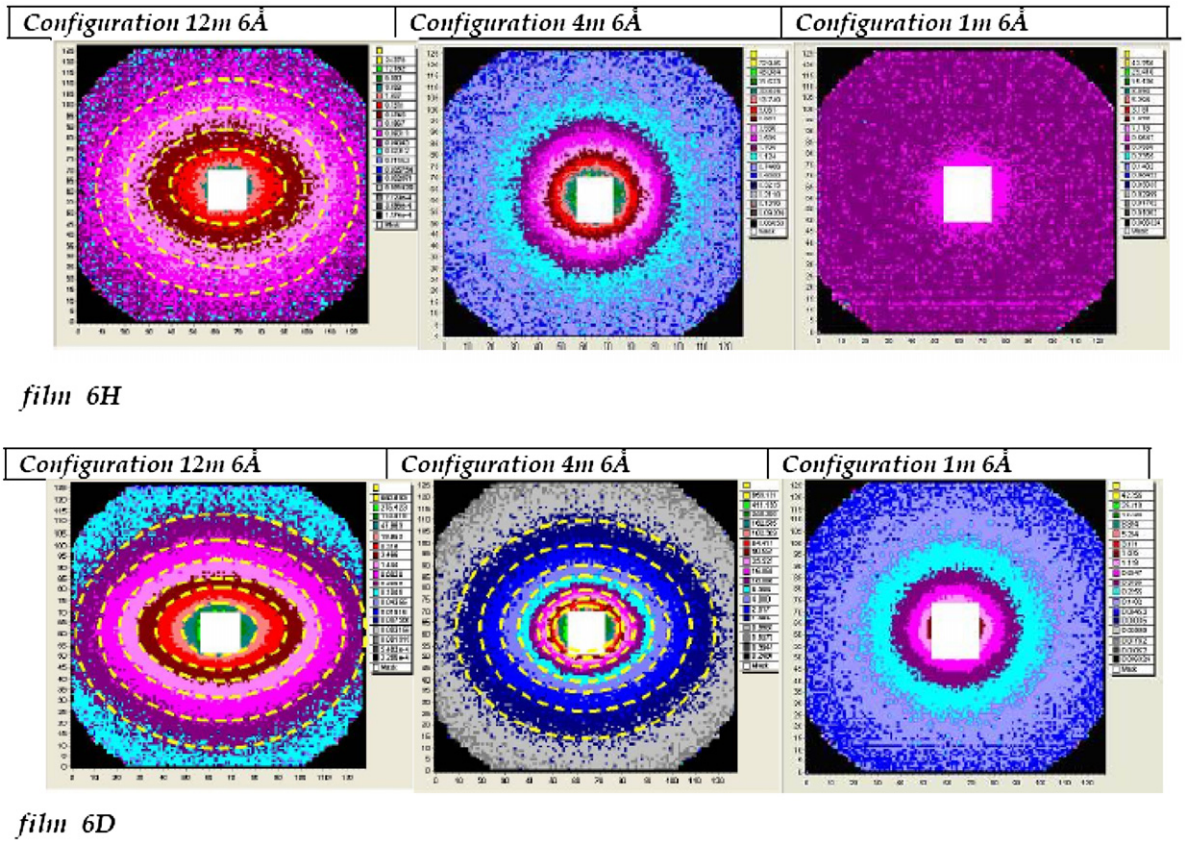

Fig. 16. Anisotropic scattering of a film made of a polymer matrix containing nanoparticles, on an X, Y multidetector located at 12, 4 and 1 m. The wavelength is equal to 6 Å for all distances, so a shorter distance corresponds to larger q range. The stretching direction of the films is vertical.
Upper: matrix made of non-deuterated polystyrene similar to the non-deuterated grafted polystyrene ones: one sees only the silica particles, which are not deformed, except for their aggregates at low q (large scales).
Lower: matrix made of deuterated polystyrene, presenting high contrast with respect to the non-deuterated polystyrene chains brought together with the particles: the scattering is dominated by the signal of these chains surrounding the particles inside the matrix, which appears anisotropic at low q and intermediate q, and isotropic at large q.

– on the upper row the 'silica only' scattering (particles in non-deuterated matrix). It is anisotropic at low q, with an elliptical shape (left-hand side image): this corresponds to deformed aggregates. On the contrary, the scattering is completely isotropic at medium and large q (middle and right-hand side images): the elementary silica nanoparticle is not deformed.
– On the lower row the polymer scattering (for the same particles in a deuterated matrix) is anisotropic at low q. This may be linked to the deformation of the global shape of the aggregates since they contain labeled chains, but also to the deformation of the chains themselves. We actually see some anisotropy also at medium q: we conclude that some of the polymer chains surrounding the particles are deformed.

To proceed further towards a quantitative comparison, we need comparison with a model. If particles were isolated with chains grafted regularly at their surface, chains would form a corona of chains. What would it give if those chains were deformed? This leads us to achieve the goal of this section: to show a calculation of the expected anisotropic scattering; we will limit ourselves here to the form factor, approached in [19]. *For the isotropic case*, the form factor of a core–corona system has been calculated, for A–B block copolymer emulsion droplets (core of solvophobic A sequences surrounded by a corona of solvophilic B sequences), by Pedersen et al. [22]. In the basic case, the core, made of a solvophobic polymer is considered as compact. Its signal is the one of a compact sphere, while the corona is made of chains swollen by the solvent. In our case of grafted silica, the core is made of silica and the grafted chains form a corona and are swollen by the matrix chains. The global form factor can be written [22]:

$$P_{\text{grafted silica}}(q) = F_{\text{hybrid}}(q) = (\Delta\rho_{\text{core}})^2.v_{\text{core}}^2.F_{\text{core}}(q) + (\Delta\rho_{\text{chain}})^2.v_{\text{chain}}^2.F_{\text{chain}}(q) + 2.N.v_{\text{core}}v_{\text{chain}}.(\Delta\rho_{\text{core}}.\Delta\rho_{\text{chain}}).S_{\text{core–chain corona}}(q) + N.(N-1)(\Delta\rho_{\text{chain}})^2.v_{\text{chain}}^2.S_{\text{chaincorona–chaincorona}}(q) \quad (19)$$

The first term is the self-correlation term of the core, i.e. its form factor. The second term is the self-correlation term of each of the N chains. The third term is the cross-term between the core and the N chains of the corona. The fourth term is the cross-term between each chain with the $N-1$ other chains of the corona. It is a convolution—thus a simple product in Fourier space—of two amplitude factors (an amplitude factor is defined by the fact that a form factor is the product of an amplitude factor by its conjugate): the global amplitude factor of the corona and the amplitude factor of one chain (here a Gaussian chain).

We have *extended* the Pedersen derivation [22] to *the deformed case* [19]: the silica core is not deformed, obviously, whereas the polymer shell is. At low q, a calculation of a simple core–corona model with deformed ellipsoidal corona would be convenient. However, at medium q, we need to calculate the contribution of the chain conformation, because its anisotropy gives a specific q dependence of the scattering anisotropy, as we will see now. From former work done at LLB, extensively, on chain conformation in melts and networks (in collaboration with J. Bastide), we know that the form or amplitude factor of stretched chains in a melt or a network is different from the one of a polyelectrolyte chain. The latter is extended by repulsion between each segment along the chain. On the reverse, in a network the chain is pulled through a few points relatively far from each other. The form factor is relatively easy to calculate. This is because the chain conformations under deformation have been extensively studied theoretically as a route to calculation of mechanical properties in amorphous polymers. We can adapt these calculations to derive the scattering. The basic model [23] is a network of chains of N_C segments at fixed end-to-end vector, to which is associated an entropy, since the number of accessible conformations is restricted to a subset of the full set of accessible conformations. Since we are in the regime of relaxation where an entangled melt behaves as a rubber, we use a network model and consider chains of sub-chains of N_e segments, with their ends bridged to other chains by temporary crosslinks. At rest, the distribution of the end-to-end vectors is Gaussian, and we recover an average Gaussian behavior. Under stretching, the distribution of the end-to-end vectors is deformed affinely to the macroscopic deformation, which is transmitted down to the size corresponding to N_e segments. Below this size, we recover progressively the isotropic Gaussian chain; this is called the 'loss of affineness' [24].

In Fig. 15 the lower and upper sets of dots (blue and green) display the measured scattering along parallel and perpendicular directions. We see that the curves join together at large q, i.e. at sizes lower than the threshold for loss of affineness. We obtain a similar behavior from the model. At low q, the chain corona is deformed, at medium q the scattering recovers isotropy when increasing q; the comparison is satisfying with the model for a stretching ratio $\lambda = 2$, equal to the macroscopic one applied to the sample. In summary, chains of the corona and close to the corona appear deformed as much as the matrix, at least at the corresponding stretching temperature, 112 °C. It is beyond our scope to discuss whether it is already too high to see a 'glassy layer': the glass transition temperature Tg is probably abated by residual solvent down to 90, even 80 °C. The aim of this discussion was simply to show the feasibility of getting interesting information in the domain of mechanical reinforcement of polymers.

6. Conclusion and final remarks

We have given above examples of how strong contrast can be varied due to the large range of scattering length density brought by deuteration, how this can be used in mixed systems by various strategies, and how it is useful to compare with nanometric scale analytical theories and simulations. The technique is mature for objects of size less than ∼500 Å, and distances between objects less than a few 1000 Å. In this range X-rays can be used, but neutrons offer the possibility of contrast. To look at larger scales, smaller scattering angles are required, which is hindered by flux problems. Presently, the possible progress is mostly in improving the neutron flux, using more sophisticated optics (supermirror guides and elliptical mirrors, multi-beam collimators, neutron lenses) and large detectors, allowing gains in recording time by factors ten or a hundred, or gains in collimation permitting to reach lower angles, thus larger scales. At these scales, the technique is competing in principle with X-rays—though only a few synchrotron facilities reach the q range below 10^{-2} Å^{-1}. Competition exists also with visible light, at very low q only. Electronic microscopy is also very important, but labelling, accuracy and non-destructive aspects are still strong advantages of the

neutron radiation. And one must never forget that the averaging brought by scattering techniques is a huge advantage in studying very complex systems.

Mixed systems are a promising field: industrial formulation is alive even more than before, since it follows a present trend of companies to get the best of products or to create new ones without too heavy new synthesis investment. New fields are under strong development, where well thought out tricks can also lead to fast progress in smaller size companies, as in biotechnology and pharmacy, which imply nanotechnology. Finally, nanotechnology combining soft matter and hard matter is slowly progressing: this will again be the occasion of creating mixed systems, and benefit of additional properties of neutrons, such as, for example, their magnetic properties.

Acknowledgements

We wish to thank colleagues from LLB: G. Jannink, J.P. Cotton, A. Brûlet, and J. Bastide, for common work on polyelectrolytes and deformed chain conformation; J. Jestin for ongoing experimental and modelisation work in nanocomposites. We thank also J.M. Verbavatz, for Freeze Fracture FFTEM on the polyelectrolytes–proteins complexes.

Appendix A. The zero average contrast method

We described in the text a way of zero deuterated fraction extrapolation of the form factor for a chain inside a given system. We give here another method, which is more direct for polymer solutions. In particular, at the LLB, the form factor of polyelectrolyte chains has been measured by this method, yielding the variation of the persistence length [25]. Let us recall the fundamentals of this very convenient method by which the form factor of a chain among others can be obtained. We start from the general expression of the scattered intensity:

$$I(q)\ (\mathrm{cm}^{-1}\text{ or }\mathrm{\AA}^{-1}) = (1/V).\mathrm{d}\Sigma/\mathrm{d}\omega = 1/V \sum_i \sum_{,j} \left\{k_i.k_j \exp\left(\mathrm{i}.q.(r_i - r_j)\right)\right\} \tag{A.1}$$

where k_i (cm or Å) $= b_i - b_s$. $(V_{\mathrm{mol}\,i}/V_{\mathrm{mol}\,s})$ is the 'contrast length' between one repeating unit i (same with j) of scattering length b_i and molar volume $V_{\mathrm{mol}\,i}$, and a solvent molecule (b_s, $V_{\mathrm{mol}\,s}$), of scattering length b_s and molar volume $V_{\mathrm{mol}\,s}$; in other words, following the formula of the main text, $k_i = \Delta\rho_i.V_{\mathrm{mol}\,i}$.

Assume first that all chains are labeled with respect to the solvent; here we dissolve H-polystyrene into D_2O. The concentration is c_p, in mole/L (or mole/Å^3), so the total volume fraction of chains is $\Phi_T = N_\mathrm{Av}.c_p.V_{\mathrm{mol}\,i}$, where N_Av is the Avogadro number. Then for all i, we have $k_i = k_\mathrm{H}$, and

$$I(q)\ (\mathrm{cm}^{-1}\text{ or }\mathrm{\AA}^{-1}) = (1/V).\mathrm{d}\Sigma/\mathrm{d}\omega = k_\mathrm{H}^2 S_T(q) \tag{A.2}$$

Using Å and Å^{-1} as the units for k_H and $I(q)$, we obtain $S_T(q)$ in Å^{-3}. Quite generally,

$$S_T(q) = S_1(q) + S_2(q) \quad (\mathrm{\AA}^{-3}) \tag{A.3}$$

where

$$S_1(q)\ (\mathrm{\AA}^{-3}) = \frac{1}{V} \sum_{\alpha,} \sum \sum_{i,j} \exp\left(\mathrm{i}.q.(r_i^\alpha - r_j^\alpha)\right) \tag{A.4}$$

corresponds to the correlations between monomers i, j of the same chain α (intrachain scattering) and

$$S_2(q)\ (\mathrm{\AA}^{-3}) = \frac{1}{V} \sum \sum_{\alpha,\beta\neq\alpha} \sum \sum_{i,j} \exp\left(\mathrm{i}.q.(r_i^\alpha - r_j^\beta)\right) \tag{A.5}$$

corresponds to the correlations between monomers i, j of two different chains α and $\beta \neq \alpha$ (interchain scattering).

Assume now that *only a fraction of the chains is labeled*. We use a mixture of a number fraction x_D of d-PSS chains ($k_i = k_\mathrm{D}$) and $(1 - x_\mathrm{D})$ of h-PSS chains ($k_i = k_\mathrm{H}$). The total volume fraction of chains in the solution is the sum of the volume fractions of the two types of chain, $\Phi_T = \Phi_\mathrm{H} + \Phi_\mathrm{D}$ (we have in general $V_{\mathrm{mol}\,H} = V_{\mathrm{mol}\,D}$, so $\Phi_\mathrm{D}/\Phi_T = x_\mathrm{D}$ and the equation $\Phi_T = N_\mathrm{Av}.c_p.V_{\mathrm{mol}\,H}$ is still valid, c_p being the total polymer molar concentration). The scattered intensity (A.1) becomes:

$$I(q)\ (\mathrm{cm}^{-1}) = (1/V).\mathrm{d}\Sigma/\mathrm{d}\omega = \left\{\left[(1-x_\mathrm{D})k_\mathrm{H}^2 + x_\mathrm{D}k_\mathrm{D}^2\right]S_1(q)\right\} + \left\{\left[(1-x_\mathrm{D})k_\mathrm{H} + x_\mathrm{D}k_\mathrm{D}\right]^2 S_2(q)\right\} \tag{A.6}$$

This second type of labeling allows us to suppress the interchain contribution $S_2(q)$, if we can have

$$(1 - x_D)k_H + x_D k_D = 0 \tag{A.7}$$

This is possible if we use as a solvent a mixture of H_2O and D_2O: then the average scattering length of the solvent b_S can be varied. In the equation above, the symmetric case $k_H = -k_D$ (which also implies $x_D = 0.5$) is the most efficient situation in term of intensity. This is obtained if b_S/V_S is made equal to the arithmetic average of $b_H/V_{\text{mol H}}$ and its pendent $b_D/V_{\text{mol D}}$. For PSS, this corresponds to a solvent constituted of 71% H_2O and 29% D_2O [8–10]. We write $|k_{ZAC}| = -k_H = k_D$, and Eq. (A.2) gives:

$$I(q) = k_{ZAC}^2 S_1(q) \tag{A.8}$$

which permits a direct measurement of intrachain scattering of one chain among the others, even in the semi-dilute regime. The values evaluated for the contrast lengths of the Na counterions with the H_2O/D_2O mixture used here are low; their contribution to the scattering have therefore been neglected. This has been confirmed by a more refined evaluation accounting for hydration [26]. The $S_1(q)$ limit at q tending to zero is

$$\lim_{q\to 0} S_1(q) = c_p.N_{Av}N_w \tag{A.9}$$

where c_p should be expressed in mole/Å^{-3}. Hence, from the definition of the form factor, we can write:

$$S_1(q) = c_p N_{Av} N_w P(q) \tag{A.10}$$

To give an order of magnitude, the zero q limit of $S_1(q)$ is close to 0.2 Å^{-3} for $c_p = 0.34$ M. This corresponds for $I(q)$ to about 10 cm^{-1}.

The ZAC technique has been used since on polyelectrolytes by other authors [17,26–28].

References

[1] J.P. Cotton (Ed.), Cours Ecole JDN Albé, J. Phys. IV France 9 (1999) 21–49, available soon on LLB website http://www-llb.cea.fr/.
[2] D. Espinat (Ed.), Application des techniques de diffusion de la lumière, des rayons X et des neutrons à l'étude des systèmes colloïdaux, Revue de l'Institut Français du Pétrole, vol. 15, Technip Ed., Paris, 1990, pp. 45–46.
[3] H.C. Benoit, J.S. Higgins, Polymers and Neutron Scattering, Oxford University Press, London UK, 1997.
[4] J. Gummel, Ph.D., Université d'Orsay Paris 11 (2006), available on LLB website, http://www-llb.cea.fr/.
[5] F. Cousin, J. Gummel, D. Ung, F. Boué, Langmuir 21 (2005) 9675–9688.
[6] J. Gummel, F. Boué, B. Demé, F. Cousin, J. Phys. Chem. B 110 (2006) 24837–24846.
[7] J. Gummel, F. Cousin, J.-M. Verbavatz, F. Boué, J. Phys. Chem. B 111 (2007) 8540–8546.
[8] J. Gummel, F. Cousin, F. Boué, JACS (Communication) 129 (18) (2007) 5806–5807.
[9] J. Gummel, F. Cousin, F. Boué, submitted for publication.
[10] (a) C.L. Cooper, P.L. Dubin, A.B. Kayitmazer, S. Turksen, Curr. Opin. Coll. Interface Sci. 10 (2005) 52–78;
(b) C. Tribet, Complexation between amphiphilic polyelectrolytes and proteins: from necklaces to gels, in: T. Radeva (Ed.), Surfactant Science Series "Physical Chemistry of polyelectrolytes", M. Dekker, 1999, pp. 687–741 (Chapter 19).
[11] (a) J.P. Cotton, D. Decker, H. Benoit, B. Farnoux, C. Picot, G. Jannink, R. Ober, J. des Cloizeaux, Macromolecules 7 (1974) 863;
(b) B. Farnoux, M. Daoud, J.P. Cotton, G. Jannink, M. Nierlich, F. Boué, J. Appl. Crist. 11 (1978) 511–513;
(c) M. Nierlich, C. Williams, F. Boué, J.P. Cotton, M. Daoud, B. Farnoux, G. Jannink, J. Appl. Crist. 11 (1978) 504–507.
[12] P. Calmettes, D. Durand, M. Desmadril, P. Minard, V. Receveur, J.C. Smith, Biophys. Chem. 53 (1994) 105–114.
[13] D. Russo, D. Durand, M. Desmadril, P. Calmettes, Physica B (2000) 276–278.
[14] (a) M. Nierlich, F. Boué, A. Lapp, R. Oberthür, Coll. Pol. Sci. 263 (1985) 955;
(b) M. Nierlich, F. Boué, A. Lapp, R. Oberthür, J. Phys. 46 (1985) 649.
[15] A. Brûlet, F. Boué, J.P. Cotton, J. Phys. II (Paris) 6 (1996) 885–891.
[16] (a) P. Sharp, V.A. Bloomfield, Biopolymers 6 (1968) 1201;
(b) J. des Cloizeaux, Macromolecules 6 (1973) 403.
[17] M.N. Spiteri, C.E. Williams, F. Boué, Macromolecules 40 (18) (2007) 6679–6691.
[18] (a) F. Carlsson, P. Linse, M. Malmsten, J. Phys. Chem. B 105 (2001) 9040–9049;
(b) F. Carlsson, P. Linse, M. Malmsten, JACS 125 (2003) 3140–3149;
(c) S. Ulrich, M. Seijo, S. Stoll, Curr. Opin. Coll. Interface Sci. 11 (2006) 268–272.
[19] A. El Harrak, Ph.D., Université Orsay Paris-Sud (2005), available on LLB website http://www-llb.cea.fr/.
[20] A. El Harrak, G. Carrot, J. Oberdisse, C. Eychenne-Baron, F. Boué, Macromolecules 37 (2004) 6376–6384.
[21] G. Carrot, A. El Harrak, J. Oberdisse, J. Jestin, F. Boué, Soft Matter 2 (2006) 1043–1047.
[22] J.S. Pedersen, C. Svaneborg, K. Almdal, I.W. Hamley, R.N. Young, Macromolecules 36 (2003) 416.

[23] (a) H.M. James, E. Guth, J. Chem. Phys. 11 (1943) 455;
(b) R.C. Ball, M. Doi, S.F. Edwards, M. Warner, Polymer 22 (1981) 1010.
[24] J. Bastide, J. Herz, F. Boué, J. Physique 46 (1985) 1967.
[25] M.N. Spiteri, F. Boué, A. Lapp, J.P. Cotton, Phys. Rev. Lett. 77 (26) (1996) 5218–5220.
[26] E. Dubois, F. Boué, Macromolecules 34 (2001) 3684–3697.
[27] Y. Zhang, J. Douglas, E. Amis, J. Chem. Phys. 114 (2001) 3299–3313.
[28] M. Heinrich, M. Rawiso, J.G. Zilliox, J.P. Simon, Eur. Phys. J. E 4 (2001) 131.